Prevention of Back Face Debris Scattering in RC Slabs Under Low-Velocity Impact Using Anchored Steel Deck Plates

Mizushima, Yasunori
Gohara, Masaki
Shimada, Ryoko
Idosako, Yuki

(Citation)
Japan Architectural Review,8(1):e70052

(Issue Date)
2025-01

(Resource Type)
journal article

(Version)
Version of Record

Japan Architectural Review

Japan Architectural Review Open Access Architectural Institute of Japan

ORIGINAL PAPER OPEN ACCESS

Prevention of Back Face Debris Scattering in RC Slabs Under Low-Velocity Impact Using Anchored Steel Deck Plates

Yasunori Mizushima[1] | Masaki Gohara[2] | Ryoko Shimada[3] | Yuki Idosako[4]

[1]Department of Architecture, Graduate School of Engineering, Kobe University, Kobe, Japan | [2]Graduate School of Human Science and Environment, University of Hyogo, Himeji, Japan | [3]Building Structure Engineering Department, JFE Metal Products Corporation, Tokyo, Japan | [4]Research and Development Institute, Takenaka Corporation, Chiba, Japan

Correspondence: Yasunori Mizushima (mizushima@bear.kobe-u.ac.jp)

Received: 16 April 2025 | **Revised:** 25 July 2025 | **Accepted:** 11 August 2025

Funding: The authors received no specific funding for this work.

Keywords: low-velocity impact | LS-DYNA | reinforced concrete slab | steel deck plate | thin slab

ABSTRACT

The low-velocity impact of thin reinforced concrete (RC) slabs by accidentally dropped objects during building construction raises safety concerns, as complete perforation and back-face debris can injure workers and third parties passing under the slabs. Various methods have been proposed to enhance the impact resistance of RC structural members, such as using high-performance materials or surface strengthening with sheets or strip materials. However, these methods may increase construction costs and procedures, making widespread application challenging. This study proposes an anchoring system for the ends of steel deck plates to suppress debris scatterings. Because steel deck plates are commonly used under RC slabs in building construction as permanent formworks or materials for composite slabs, this system is cost-effective and straightforward. A half-scaled impact test was performed to compare specimens with and without the anchoring system, validating its effectiveness in suppressing debris scatterings. Additionally, a component pull-out test and a finite element analysis were conducted to explore the anchoring system's behavior, followed by an impact analysis considering the pull-out of the anchoring system based on the results of component tests and analyses. The analysis replicated the variation in deck plate detachment behavior with and without the anchoring system.

1 | Introduction

In urban construction, the threat of falling objects during building processes is a significant risk, particularly when the construction site is located above public thoroughfares. If such objects breach the underlying slabs, severe fatalities could occur to construction workers and users of these passageways alike. Night work is often employed to mitigate these risks, albeit at the cost of increased expenses and project delays. This practice hinders the optimal utilization of valuable urban spaces located above public pathways. However, if reinforced concrete (RC) slabs are designed to withstand the impact of falling objects, construction can proceed safely without resorting to night work. This not only enhances public safety but also reduces costs and shortens project timelines. Therefore, assessing the impact resistance and perforation capacity of RC slabs against falling objects is crucial for public safety and urban development.

While the behavior of RC slabs under low-velocity impact loading has been extensively investigated, most studies have focused on relatively thick slabs and overlooked the influence of reinforcement bars on penetration resistance. Ito et al.

conducted impact tests, including low-velocity impacts, on RC slabs with thicknesses similar to the projectile diameter and proposed scabbing and perforation limits [1]. In an empirical formula proposed by Degen [2], a well-known perforation limit, RC slabs with thicknesses of half the projectile diameter are within the applicable range [2]. Studies on low-velocity impacts on RC slabs with thicknesses similar to or approximately half of the projectile diameter have been reported [3–8]. Although Şengel et al. investigated the low-velocity impact behavior of RC slabs emphasizing the impactor geometry, the RC slabs' thickness exceeded half of the projectile's diameter [3]. Xiao et al. conducted a low-velocity impact test considering the projectile diameters, with the minimum slab thickness set at half the widest projectile diameter [4]. Wang et al. conducted hard projectile impact tests on RC slabs, albeit not at low velocities, owing to the smaller projectile diameters used in previous studies compared with those in their assumed impact scenario. However, the maximum slab thickness in their tests was only half the projectile diameter [5]. Wang et al. numerically analyzed the low-velocity impact of pre-stressed concrete slabs in which the projectile diameter matched the slab thickness [6], with reference to experiments conducted by Iqbal et al. [9–11].

Considering accidentally falling objects during construction, Mizushima et al. conducted comprehensive full-scale low-velocity impact tests and finite element analysis (FEA), proposing a perforation prediction method considering the effect of reinforcements [12, 13]; they concluded that debris scattering and steel deck plate detachment occurred when the impact conditions were beyond the perforation limit proposed by Degen [2]. Such debris scatterings pose a threat to individuals occupying spaces beneath damaged slabs. Therefore, damage-suppression methods for RC slabs that can prevent debris scattering are desired for low-velocity impacts.

Previous studies on damage mitigation to RC structures, including slabs under impact loading, can be broadly categorized into those utilizing high-performance materials for RC slabs, those utilizing methods in which reinforcing materials are attached to the surface of slabs, and a combination of both approaches. In the first category, Othman performed a drop-weight impact test on RC plates utilizing a fiber-reinforced high-strength concrete material [14]. Curbach et al. tested the resistance of RC slabs to impact loads using carbon textiles as additional reinforcement [15]. Furthermore, numerous studies have utilized high-strength materials and those incorporating short fibers into concrete [16–22]. To illustrate the second category, Almusallam et al. tested the effect of strengthening on RC slabs utilizing carbon fiber-reinforced polymer (CFRP) sheets [23]. Similarly, Yılmaz et al. conducted impact tests on RC slabs with reinforced bonding CFRP strips on the surface [24]. Moreover, various studies have been conducted on RC slabs with surface reinforcement using different materials [25–30]. Soltani et al. and Almusallam et al. investigated a combination of fiber-added high-performance concrete and surface strengthening techniques [31, 32].

Although the utilization of high-performance materials and surface strengthening enhances the impact resistance of RC slabs, cost and practical construction remain a challenge. Fibers utilized in high-performance concrete increase material costs and make concrete handling challenging. Surface reinforcement also increases material cost and requires an additional construction procedure for bonding, making the application of these materials challenging for use in large-scale buildings with wide floor slabs.

This study proposes a novel anchoring system for steel deck plates to suppress debris scattering of RC slabs under low-velocity impact. Unlike the aforementioned techniques, this approach leverages the steel deck plates already commonly used as permanent formworks or composite slab materials, eliminating the need for specialized additional reinforcements. This method minimizes additional costs and disruptions to construction procedures onsite, as steel deck plates are commonly utilized in practical construction. To the best of the authors' knowledge, no previous studies have explored enhancing impact resistance by anchoring these widely used deck plates. The anchoring system involves folding up the ends of steel deck plates and anchoring them to the concrete, preventing debris scattering and detachment of the steel deck plate under the RC slabs. A half-scaled impact test of RC slabs was conducted with varying falling heights, with and without an anchoring system to validate the effectiveness of the proposed system. A component test and FEA of the anchoring system were conducted to examine the mechanical properties of the anchoring system. Furthermore, an FE model that could determine the debris scattering of the proposed RC slabs was developed by applying an adhesion model based on an investigation of the anchoring system to the ends of the steel deck plates.

2 | Impact Test

A half-scale impact test was conducted to assess the impact of an anchoring system on deck plate falling and debris scattering. The test specimen was designed to simulate rectangular one-way slabs found in steel framing buildings in Japan, supported by steel beams and pin bearings. Projectiles were suspended by cranes and released to fall freely onto the slabs, with the main experimental parameters being the presence or absence of the anchoring system and the impact velocity adjusted by the projectile's falling heights.

2.1 | Specimen

The dimensions of the RC slabs utilized in this study are shown in Figure 1. The study used 75 mm thick RC slabs, which are half the thickness of the 150 mm slabs used in general steel-frame buildings in Japan. The slabs were one-way with a 1150 mm support span that was supported by steel beams with an H-194×150×6×9 section and a length of 3 m. The two beams supporting the RC slabs were connected by twist-resisting joists with bolted joints to suppress beam rotation in the axial direction. The RC slab was connected to the steel beams using headed studs specified in JIS B1198, arranged in two rows 125 mm apart and connected through burnout plug welding. In typical steel-frame building construction in Japan, reinforced concrete (RC) floor slabs are commonly anchored to steel beams using headed studs. This method is widely

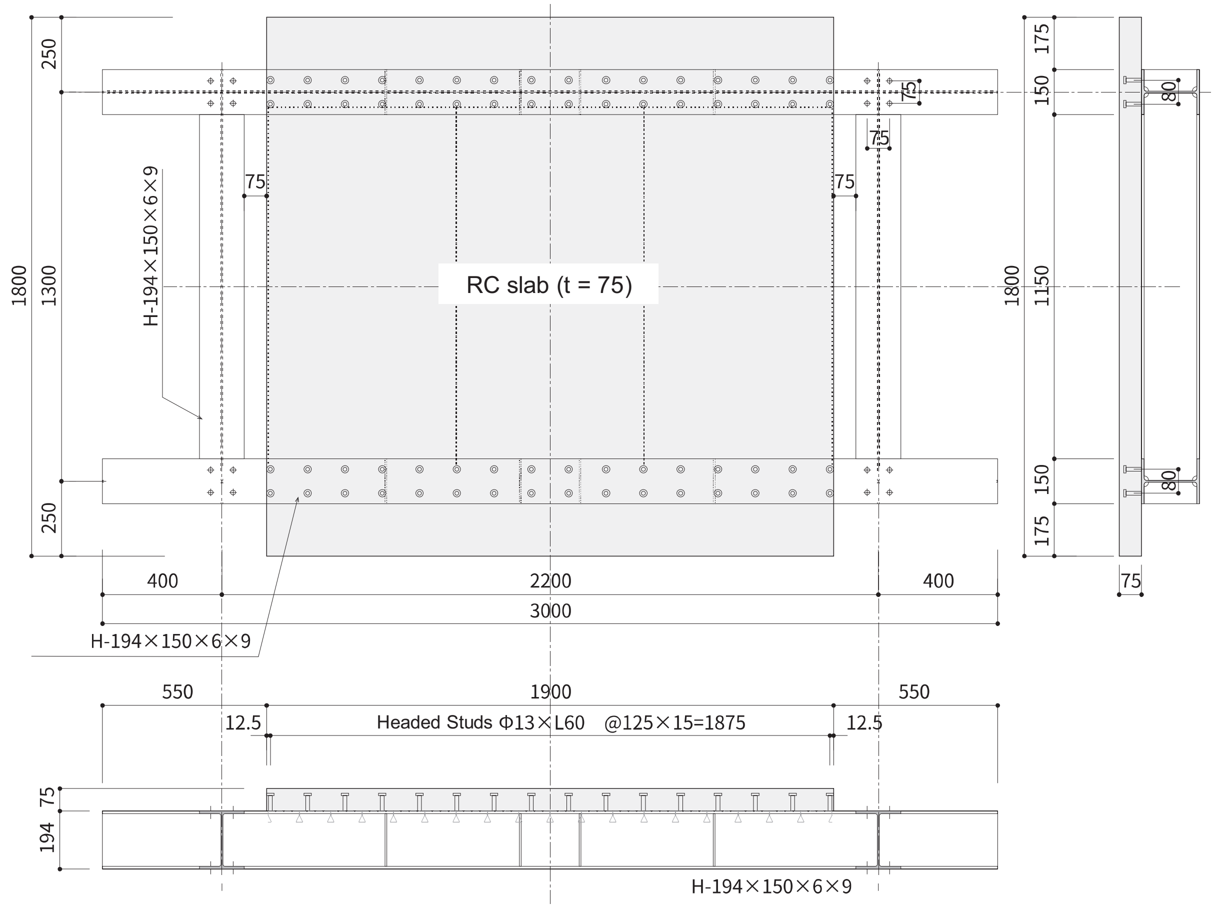

FIGURE 1 | Specimen (reinforced concrete slab) (mm).

adopted to ensure structural integrity and to simulate realistic boundary conditions. The configuration used in this study, where the RC slab is fixed to the H-beam steel girders via headed studs, is thus reflective of current engineering practice.

The reinforcement arrangements are shown in Figure 2. The reinforcement ratio of the specimens was similar to that of the specimens in Ref. [12]. The upper reinforcement bars were set with the D6@75 main and D6@100 distribution reinforcements, with the lower bars set with the D6@100 main and D4@60 distribution reinforcements.

Half-scaled steel deck plate models were installed beneath the concrete as permanent forms. Comprehensive deck plates utilized in practical buildings are made from a 1.2 mm thick steel plate by roll forming and feature triangular ribs with a height of 75 and 210 mm intervals, as shown in Figure 3. Because half-scale deck plates are challenging to produce in the roll forming process, a half-scale deck model for the specimen was created by bending 0.6 mm thick steel plates and joining them with screws and connection plates, as shown in Figure 4. Each deck plate model was constructed from six units of bent and formed plates. The anchoring system was established by folding up the ends of the deck plate models. Conceptual diagrams of unfolded and folded ends of the deck, and a photograph of the anchoring

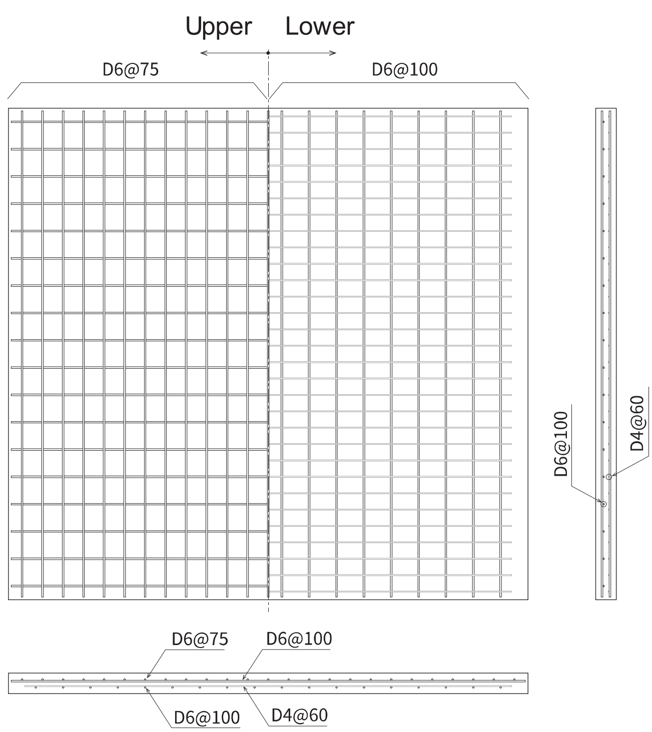

FIGURE 2 | Arrangement of reinforcement bars (mm).

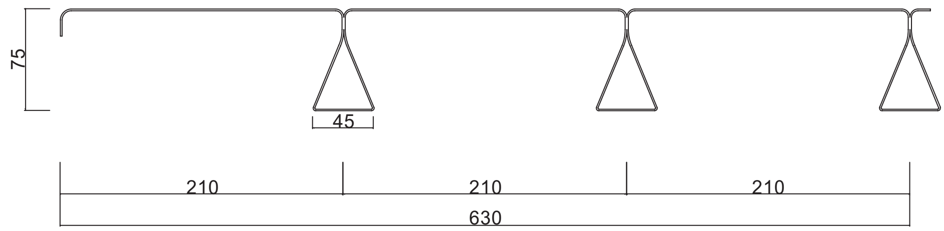

FIGURE 3 | Full-scale deck plate (mm).

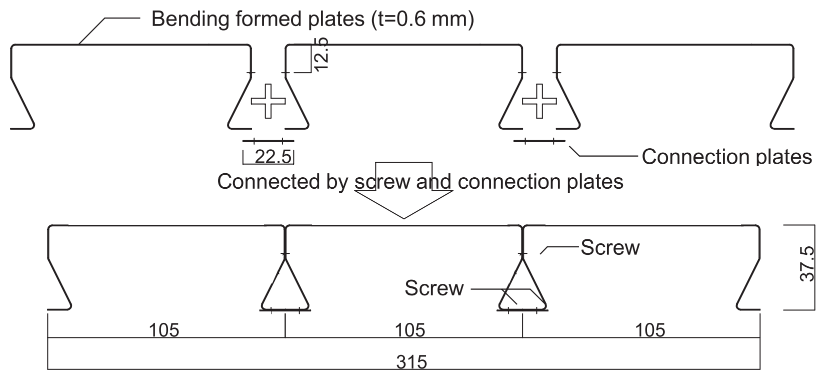

FIGURE 4 | Deck plate model used for specimens (mm).

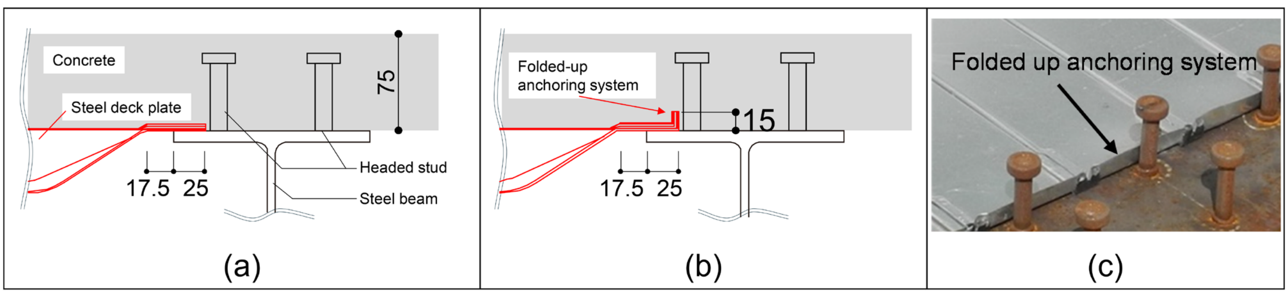

FIGURE 5 | Ends of deck plate model: (a) Without anchoring system, (b) with anchoring system, (c) photograph of anchoring portion (mm).

portion are shown in Figure 5. To prevent interference with the reinforcement bars, the length of the folded part was set equal to the cover thickness of the RC slab (15 mm) with a bending angle of 90°. The projectile, shown in Figure 6, was a square-shaped steel tube with a section of □-375 × 375 × 25 and a length of 1050 mm, weighing 318.8 kg including a suspended steel jig and wire.

The material test results of steel and concrete parts are shown in Table 1. These tests were conducted in advance for steel parts, including reinforcement bars, deck plates, and frame, with the names of the specimens provided in Section 2.3.

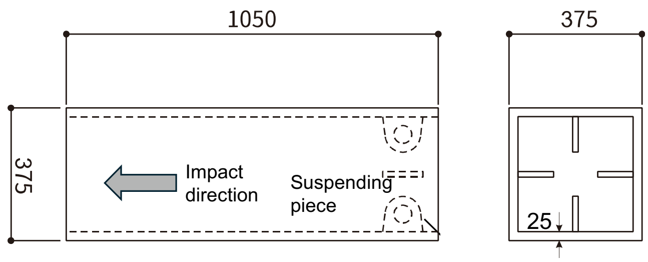

FIGURE 6 | Projectile (mm).

2.2 | Setup

In this study, an RC slab was positioned on the test stand, and the projectile was raised to a predetermined height using a rafter crane before being dropped onto the center of the slab.

The installation of the specimen is shown in Figure 7, with a photograph of the setup shown in Figure 8. A 22 mm thick steel plate mat was laid on the ground, and two H-shaped steel beams were installed on the steel plates as ground beams of the test stand. The specimens were supported by spherical bearings, sandwiched between two steel plates, with sliding sheets allowing for the translation of supporting points along the longitudinal direction to the beams, as shown in Figure 9.

The projectiles were lifted and dropped freely using a rafter crane. A plumb line was utilized to measure the predetermined impact position and falling height (distance from the top surface

TABLE 1 | Material test: (a) Steel parts, (b) concrete parts.[a]

(a)		
Parts	**Yield stress (MPa)**	**Tensile strength (MPa)**
Reinforcement, D4	382[b]	535
Reinforcement, D6	389[b]	599
Steel beams	314	452
Deck plate	296	356

(b)			
Specimen	**Young modulus (×10^4 MPa)**	**Compressive strength (MPa)**	**Split tensile strength (MPa)**
N-7.5, N-9	2.64	34.5	2.23
N-13, F-13, F-14, F-15	3.18	39.7	2.62

[a]Failure strain parameters used in the FE model are given in Section 4.1.
[b]0.2% offset yield strength.

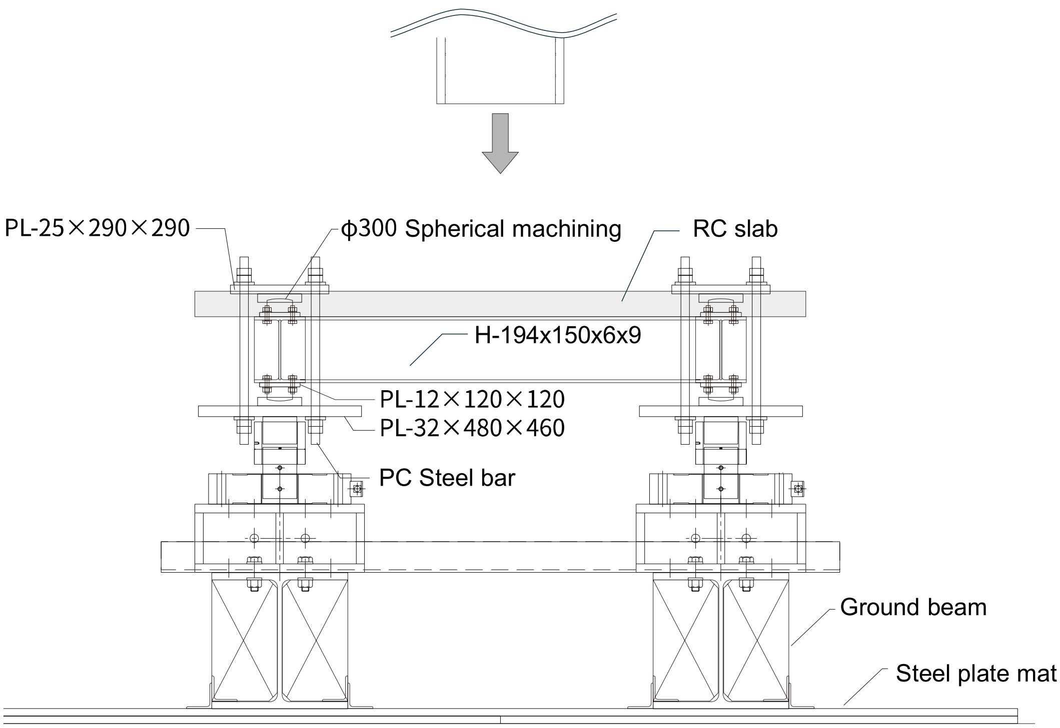

FIGURE 7 | Specimen setup.

of the RC slabs to the bottom of the projectile). The impact velocity was determined through image analysis of the footage captured using a high-speed camera. Markers were placed at the bottom end of the projectile at 200 mm intervals to avoid detection errors, as shown in Figure 8.

2.3 | Experimental Scenarios

The key experimental variables included the presence or absence of the anchoring system and the impact velocity, which was controlled by adjusting the projectile's falling height. A summary of the designed falling heights with and without the anchoring system is presented in Table 2. The experimental scenarios were named by combining a character indicating the presence or absence of the anchoring system and a number representing the falling height. The first character of the experimental scenario name can either be "N" indicating no anchoring system or "F" indicating an anchoring system. For example, N-7.5 signifies a test conducted on a specimen with no anchoring system, with a designed falling height of 7.5 m.

The falling height was set to a lower limit value, which was believed to cause deck plate detachment and debris scattering in cases without an anchoring system. Debris scattering and detachment of the deck plates of RC slabs can be identified using the perforation limit proposed by Degen [2] in cases without anchoring systems [12, 13], as expressed in Equation (1). Although

FIGURE 8 | Photograph of the setup.

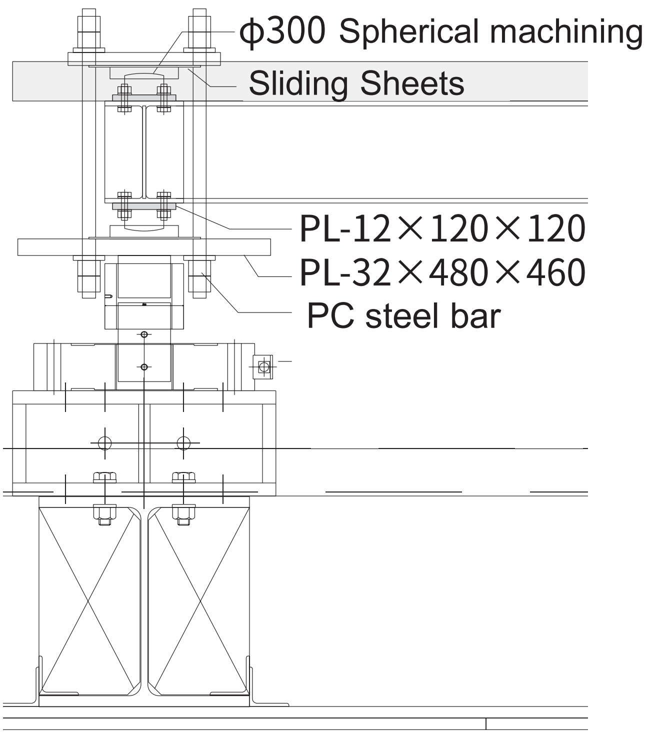

FIGURE 9 | Detail of supporting points.

TABLE 2 | Experimental scenarios.

	Designed falling height (m)				
Anchoring system	**7.5**	**9**	**13**	**14**	**15**
No	N-7.5	N-9	N-13	—	—
Yes	—	—	F-13	F-14	F-15

Degen's formula was derived for plain RC slabs, previous studies by the authors [12, 13] indicate it is applicable as an indicator of deck plate detachment in RC slabs with steel deck plates when no anchoring system is provided.

$$e = \alpha_p \left\{ 2.2\left(\frac{X}{d}\right) - 0.3\left(\frac{X}{d}\right)^2 \right\} \cdot d \tag{1}$$

where e(m) represents the perforation limit thickness proposed by Degen and X(m) represents the penetration depth calculated using the modified NDRC (Equation 2) [33], α_p represents the reduction factor specified based on the properties of the projectile for the perforation limit, and d represents the diameter of the projectile. The diameter of the projectile can be equated to that of a circle with the same perimeter as that of the rectangular steel tube [12, 13].

$$\frac{X}{d} = \alpha_c \cdot 0.01233\left\{ f_c'^{-0.5} \cdot MN \cdot d^{-2.8} V^{1.8} \right\}^{0.5} \tag{2}$$

where α_c represents the reduction factor for penetration depth, f_c' represents the uniaxial compressive strength of concrete, N represents the shape factor of a projectile, and V represents the impact velocity.

The detachment limit of the deck plates and debris scattering limit were calculated to be 7.5 m by utilizing Equations (1) and (2) for the full-scale RC slabs utilized in general steel-frame buildings, with a design strength of $f_c' = 30$ MPa. Muto et al. suggested a proportionality law for damage conditions of RC slabs in impact test [34–36]. The experimental parameters in this study were determined based on test calculations for full-scale slabs. Experiments were conducted at a design drop height of 13 m, with and without the anchoring system to validate the effectiveness of the anchoring system.

2.4 | Experimental Results

At the same falling height, the deck plate fell, and debris was scattered in the case with no anchoring system; whereas debris scattering and deck plate detachment were suppressed in the case with an anchoring system. This highlights the effectiveness of the anchoring system in suppressing debris scattering and deck plate detachment. In the experimental results described below, the actual falling heights (h) were calculated from the impact velocity (v) observed by the high-speed camera and gravity acceleration (g) using Equation (3).

$$h = v^2 / 2g \tag{3}$$

The penetration depths represent the distances between the surfaces of the remaining concrete in the impacted and surrounding parts. The penetration depth was measured by subtracting the cover concrete thickness from the distance between the surrounding concrete surface and the exposed reinforcement bars when the concrete of the impacted parts was destroyed.

2.4.1 | Without Anchoring System

The damage and deck-end dislodgement states of the N-series without an anchoring system are shown in Figures 10–13. In all the N-series scenarios, local damage of the RC slabs

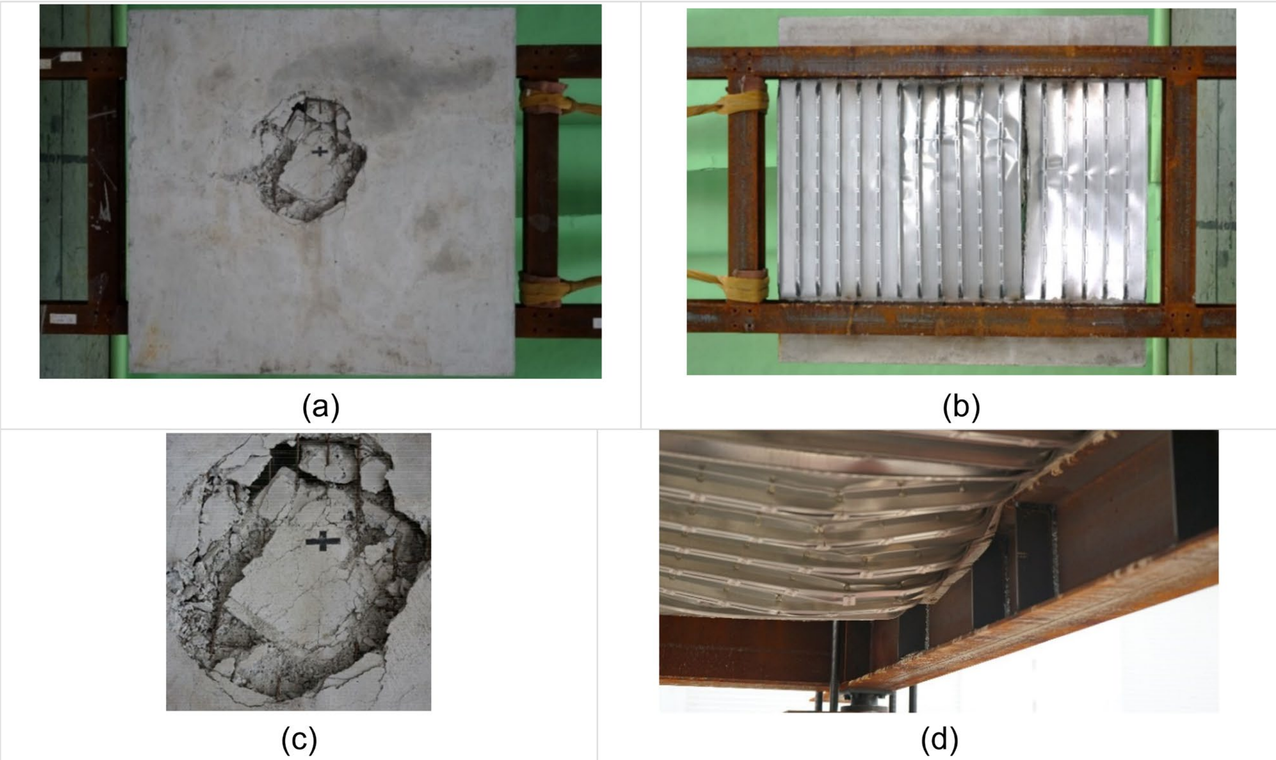

FIGURE 10 | N-7 damage stats: (a) Impact face, (b) back face, (c) close view of the impact area, (d) falling out of the end of the deck plate.

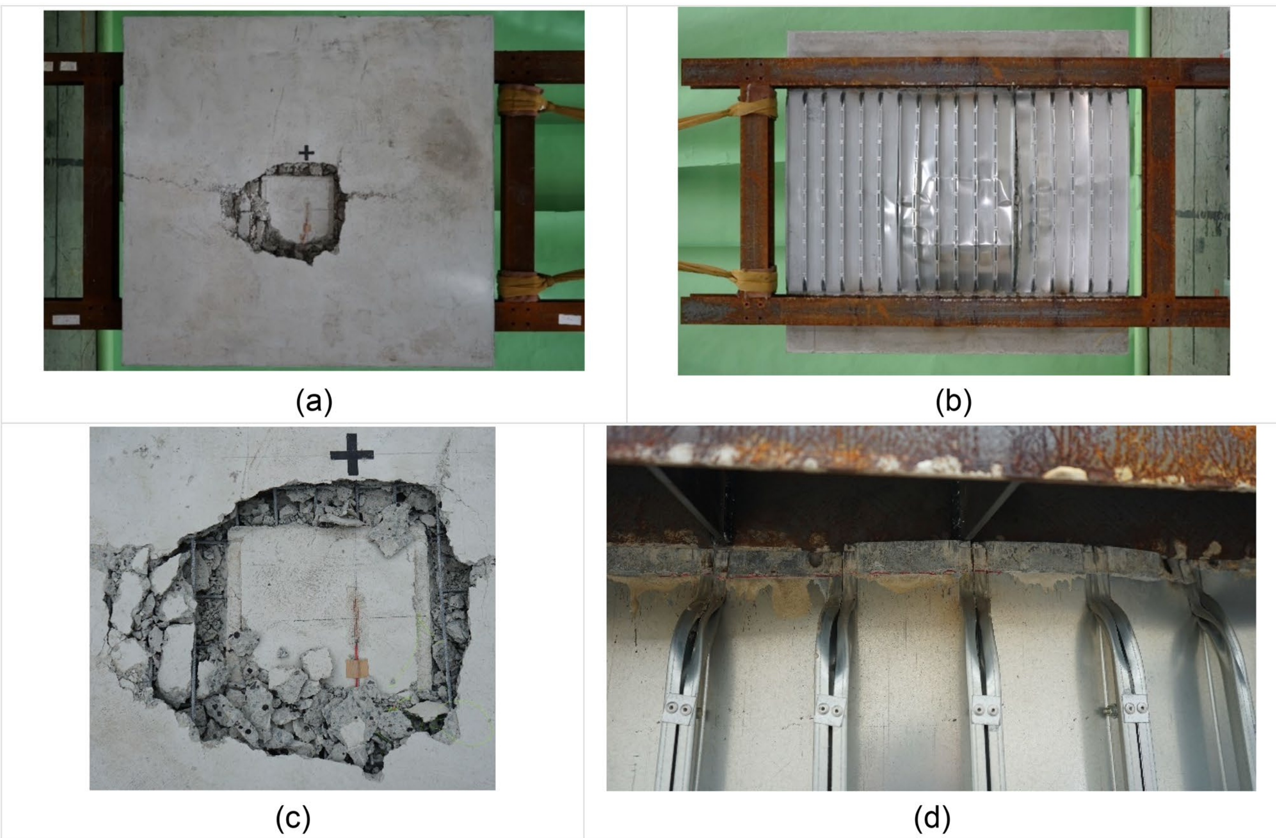

FIGURE 11 | N-9 damage stats: (a) Impact face, (b) back face, (c) close view of the impact area, (d) falling out of the end of the deck plate.

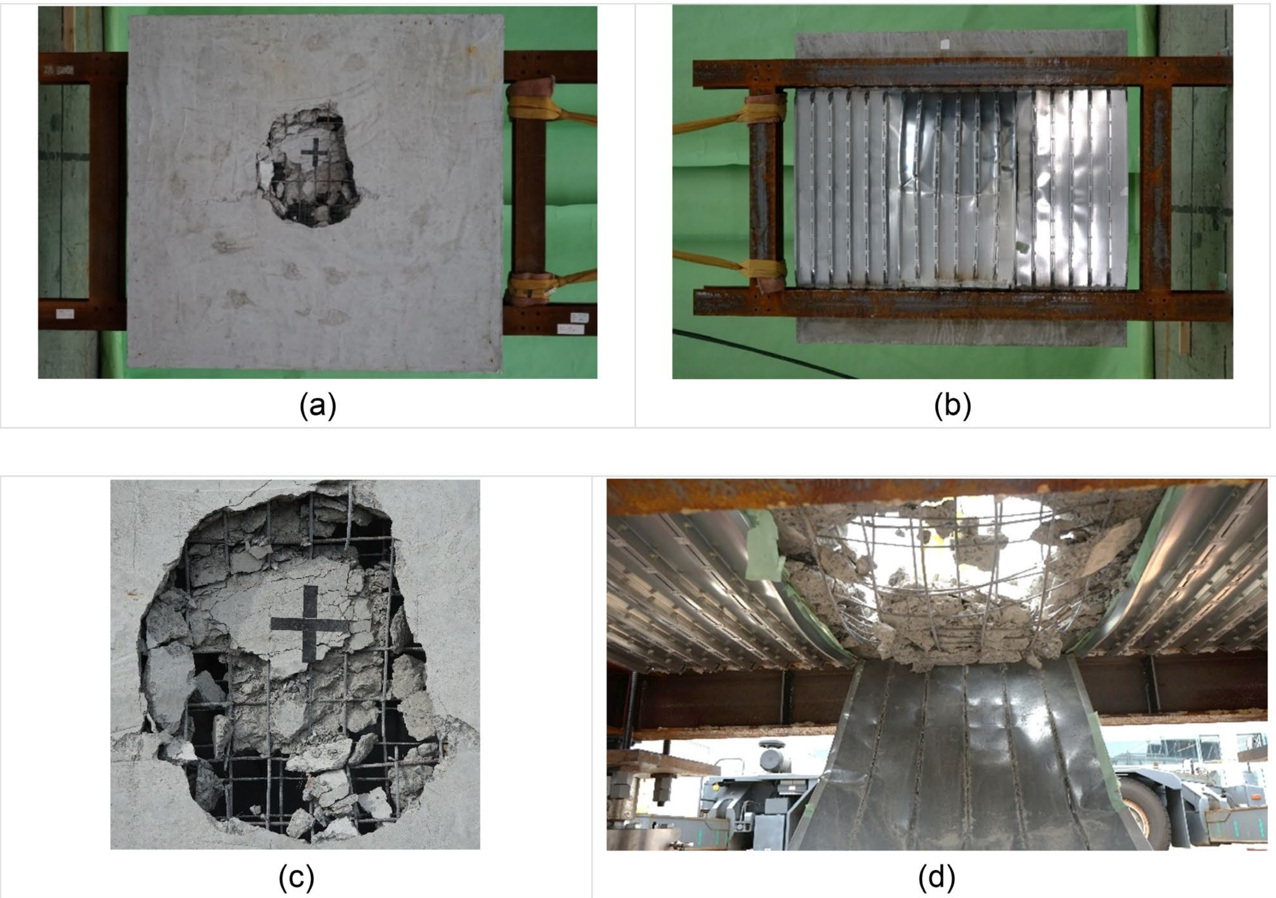

FIGURE 12 | N-13 damage stats: (a) Impact face, (b) back face, (c) close view of impact area, (d) falling out of the end of the deck plate.

was observed, and detachment of the deck plates and debris scattering were evident. Although no dedicated sensors were employed, the deck plate deformations and damage (e.g., fractures near screw connections, dislodgement amounts) were recorded through post-test inspections and photographic evidence.

For N-7.5, the actual falling height calculated from the impact velocity measured using a high-speed camera was 7.6 m, closely matching the expected experimental condition. The penetration depth was 43 mm, with a slight fall at one end and debris falling from that area. Fractures of the deck plate were observed at parts connected by screws, a phenomenon that would not occur in full-scale impact situations owing to the absence of screws.

In N-9, the calculated actual falling height was 9.1 m, close to the expected experimental condition. The penetration depth was 60 mm—closer to the thickness of the slab. One end of the deck plate fell, with debris scattering similar to that of N-7.5. At the other end of the deck, a 10 mm dislodgement was observed, and one upper reinforcement bar fractured at the impacted part.

In N-13, the actual falling height was 13.0 m, with a penetration depth of 105 mm, significantly exceeding the specimen's thickness. One end of the deck plate was removed, causing the deck plate to fall out from the RC slab, with debris scattering downwards. On the other end, a maximum dislodgement of approximately 10 mm was observed. The screw connection parts of the deck plates experienced fractures, similar to those of the other N-series specimens. Additionally, at the impact point, four upper and three lower reinforcement bars fractured.

2.4.2 | With the Anchoring System

The conditions of the RC slabs and deck dislodgement at the end of the impact tests for the F-series are shown in Figures 13–15. As with the N-series tests, the F-series examinations recorded deck deformations and fractures through post-test inspections and photographic documentation. The impact tests for the F-series showed that the anchoring system effectively prevented deck falling and debris scattering, with no deck falling out in specimens F-13 and F-14, and the first instance of dislodgement in specimen F-15, validating the effectiveness of the anchoring system. Additionally, no complete perforation of the falling object was observed in any of the cases.

F-13 experienced a slightly higher impact velocity than anticipated owing to a calculated falling height of 13.4 m and a penetration depth of 93 mm, exceeding the RC slab thickness. Deck dislodgement was suppressed, and debris scattering was not observed. The deck ends experienced a maximum displacement of 30 mm, and fractures were observed near screw connections.

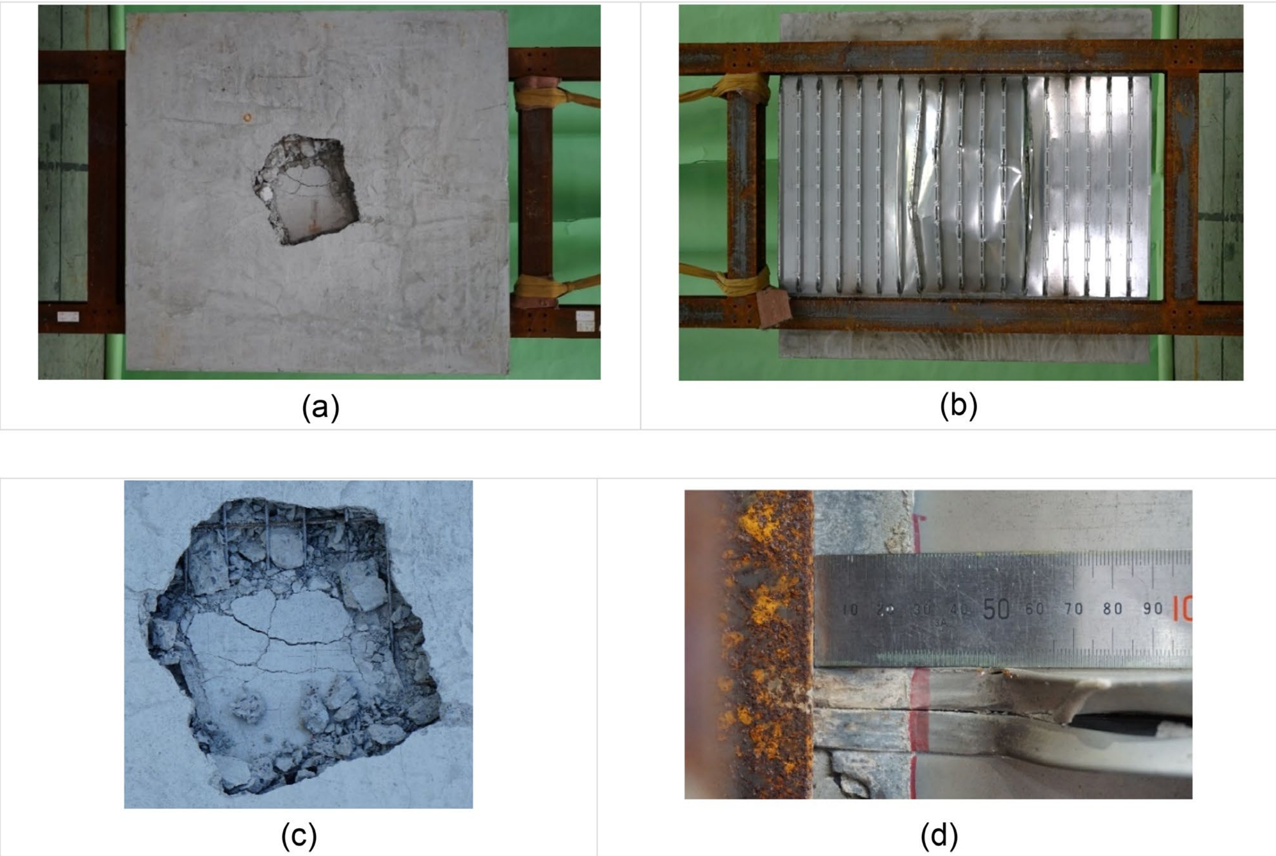

FIGURE 13 | F-13 damage stats: (a) Impact face, (b) back face, (c) close view of the impact area, (d) falling out of the end of the deck plate.

In specimen F-14, the calculated actual falling height was 13.9 m, closely matching the anticipated impact conditions. The penetration depth at the impact surface was 77 mm, which was less than that observed in F-13. The projectile impacted at a slight angle, resulting in more dispersed damage to the RC slab. This reduction in penetration depth is attributed to the dispersion of the impact energy from the angled impact. No deck dislodgement occurred, and debris scattering was suppressed. The maximum dislodgement was approximately 10 mm, with fractures observed near the screw connections and some fractures extending into the flat areas of the deck.

In specimen F-15, the calculated actual falling height was 15.7 m, resulting in a higher impact velocity than anticipated. The penetration depth at the impact surface was 177 mm. The deck was significantly dislodged, with debris scattering downward. The deck plate panel was completely fractured, seemingly initiated from a screwed area.

3 | Investigation of Mechanical Property of Anchoring System

The proposed anchoring system for RC slabs is simulated using FEA, requiring an understanding of its mechanical properties. A static pull-out experiment and FEA, considering the strain rate effect of steel material, are described to investigate its behavior during impact.

3.1 | Static Pull-Out Test

3.1.1 | Specimen and Setup

The specimen utilized for the pull-out test, fabricated by modeling an actual scale anchoring system, is shown in Figure 16. Steel plates (referred to as base plates hereinafter) and concrete were placed at both ends of the 960 mm-long deck plate. The concrete, with widths of 450 and 210 mm and a thickness of 150 mm, represented the floor slabs commonly utilized in actual buildings. To approximate the structure near the deck ends, the concrete was extended 50 mm from the base plates toward the center of the specimen. The concrete was enclosed on all sides by formwork constructed from steel plates. The formwork plates perpendicular to the pull-out direction were reinforced with two additional plates to prevent a bending failure of the concrete owing to eccentric bending caused by deck pull-out. The reinforcing and base plates were welded. The deck-end width was narrowed at the center, corresponding to the concrete widths, such that pull-out occurred at 210 mm. The ends of the deck plate were bent upward at a 90° angle by 30 mm. Notably, the deck was not welded to the base plates.

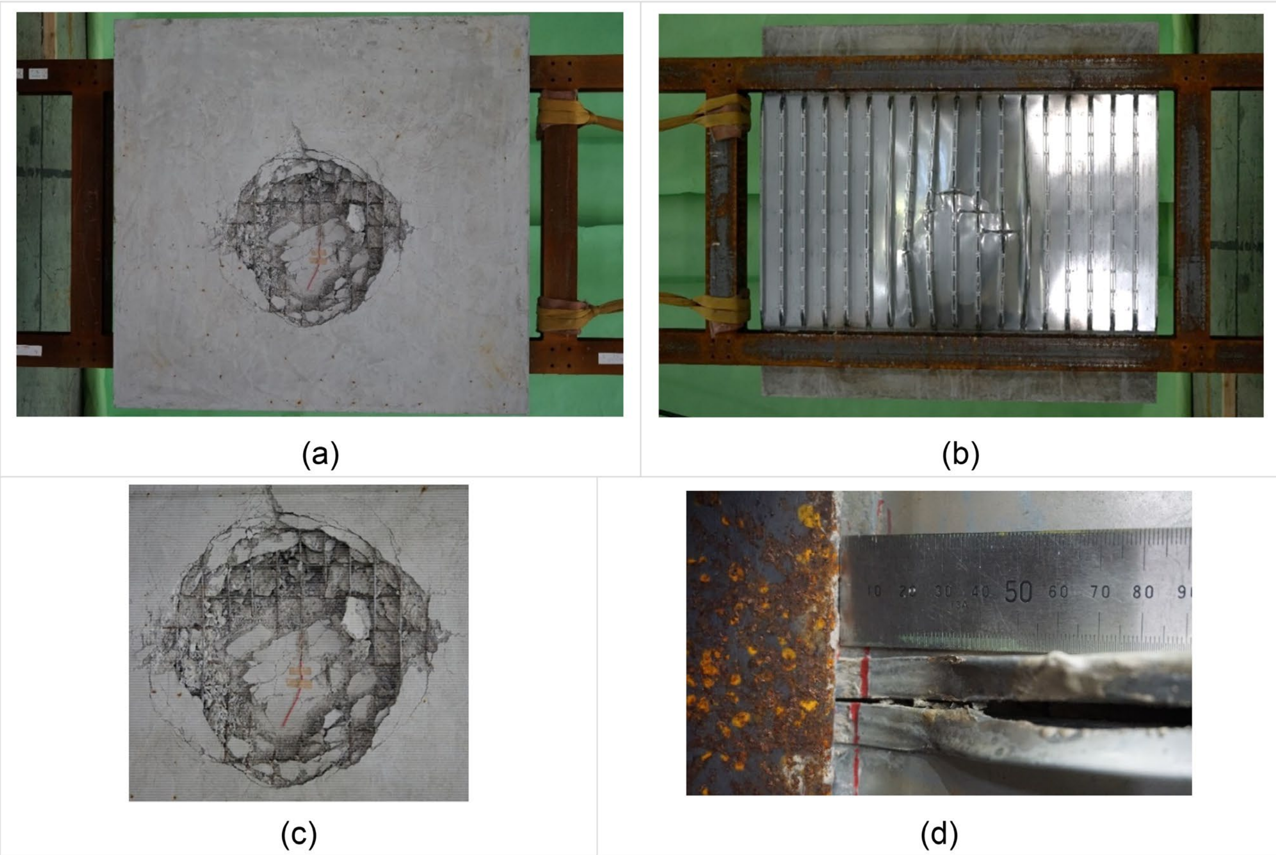

FIGURE 14 | F-14 damage stats: (a) Impact face, (b) back face, (c) close view of the impact area, (d) falling out of the end of the deck plate.

The material test results are listed in Table 3. Tests for steel materials, excluding the deck plate, were omitted as these steel parts were not expected to yield.

The experimental setup is shown in Figure 17, involving a tensile testing machine, with the deck pulled out statically from the top. The reaction force and displacement of the deck were recorded, with displacement gauges attached to both surfaces and undersides to measure the relative displacement between the deck and the base plates.

3.1.2 | Results

A reaction force and relative displacement diagram, shown in Figure 18, revealed that a maximum strength of 41 kN was achieved after pulling out approximately 5 mm. Subsequently, the load gradually decreased downwards, resulting in complete pull-out. Notably, the gradient of the diagram appeared to slightly vary after pulling out approximately 30 mm, corresponding to the fold-up length. The conditions of the specimen at the maximum load and after complete pull-out are shown in Figure 19. After complete pull-out, the folded portion of the deck plate exhibited the same elongated shape in both the impact test and the full-scale pull-out component test, confirming geometric similarity between scales. At the maximum load, a slight crack originating from the tip of the deck plate-embedded part was observed. However, no significant damage to the concrete was observed at the maximum strength or after pull-out. Following the pull-out, the end of the deck plate was completely elongated. The maximum strength in this test may be attributed to the behavior of the folded deck plate.

3.2 | Pull-Out FEA Considering Strain Rate Effect

The anchoring system's mechanical properties were investigated under static conditions; however, dynamic conditions during impact led to an FEA considering the strain rate effect of steel material for the deck plate. The analysis comprised press forming of the enclosed ends of the deck plate, the folding process to create the anchoring part, and pull-out analyses. The shape of these three stages was carried over in the analysis, whereas stresses and strains were not. The FEA was performed using LS-DYNA.

3.2.1 | Press-Forming Analysis of the Deck End

Rib pressing and forming processes were simulated using FEA to reproduce the shape of the enclosed deck end. The modeling range of the deck plate was set to 210 mm, centered on the rib, similar to that of the pull-out test specimen, as shown in Figure 20. The deck plate was modeled using Belytschko-Tsay shell elements, with a mesh size of approximately 0.5 mm and a total of 237 166 elements, determined through a trial-and-error process to identify the maximum size that would prevent excessive mesh distortion during the forming process. Six integration points were used in the sectional direction to accurately represent large bending deformations.

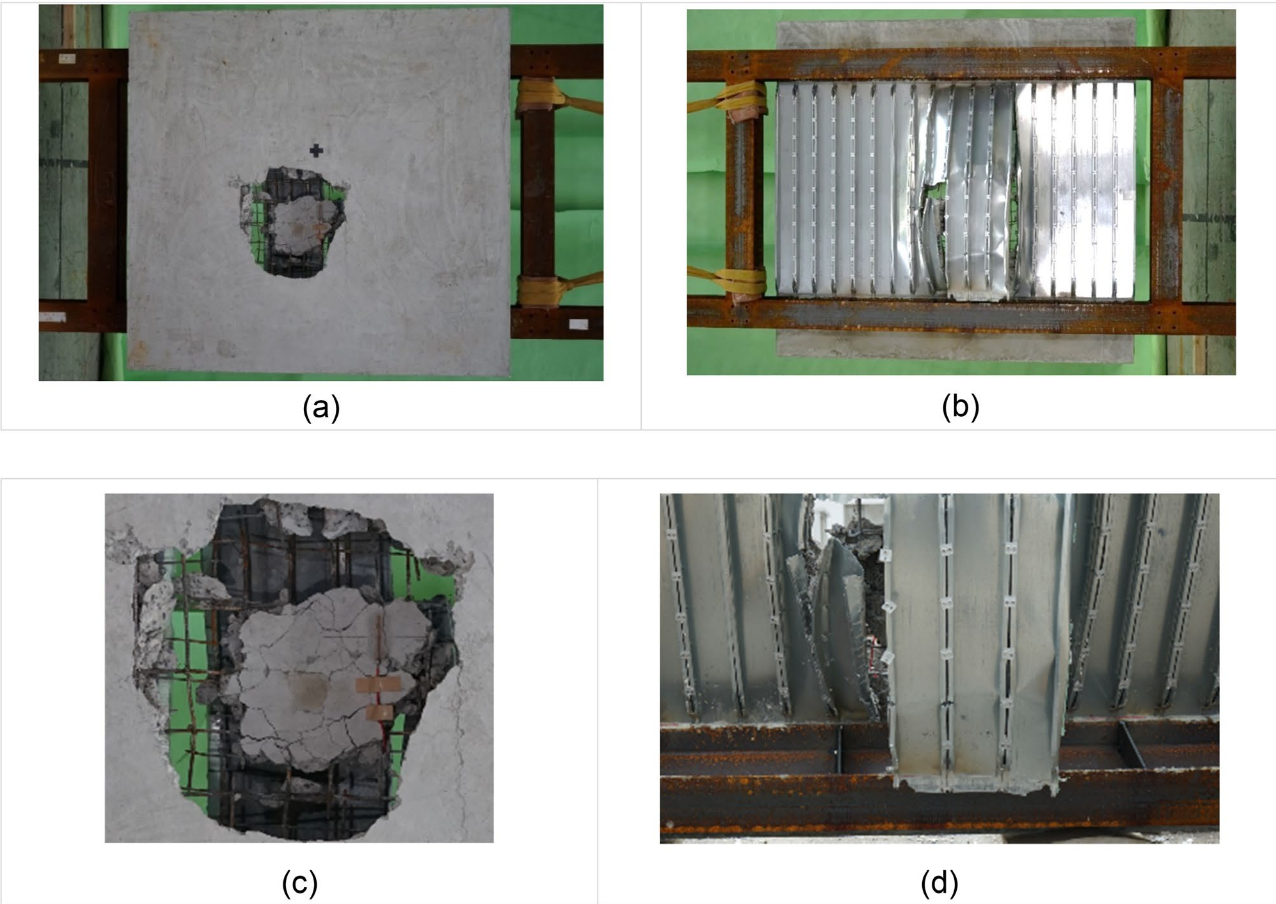

FIGURE 15 | F-15 damage stats: (a) Impact face, (b) back face, (c) close view of the impact area, (d) falling out of the end of the deck plate.

The analysis model comprised the deck plate shown in Figure 21, base plate, suppressing plates to hold the deck plate in place, pressing plate simulating the contact part of the pressing machine, and cam slider to maintain the shape of the triangular rib. The base and suppressing plates were modeled using shell elements, whereas the pressing plate and cam slider were modeled using solid elements. All components except the deck plate were modeled as rigid bodies. A perfectly elastic–plastic model, which is called *MAT_PLASTCIT_KINEMATIC, was utilized as the deck plate, with the material parameters determined from the material test listed in Table 3a.

The contact conditions based on the penalty method were established between each component, with a self-contact condition set for the deck plate owing to the pressing procedure (Figure 22). The frictional coefficient was set to 0.0 primarily to simplify the contact conditions and ensure stable convergence during the initial geometry formation stage. Since the purpose of this analysis is solely to obtain the initial shape, rather than to investigate detailed force responses, introducing friction was deemed unnecessary. The clearances between the deck and cam slider were 1.2, 3.6, and 4.2 mm at the bottom, rise, and top, respectively. The deck and suppression plates were presumably in contact with the initial conditions.

The boundary conditions for the end-press-forming analysis are shown in Figure 22. The suppression plates and cum slider were fully constrained, and a forced motion in the Z-direction was applied to the pressing plate to replicate the pressing process. Apart from Z-translational displacement, the motions of the pressing plate were constrained. Symmetrical boundaries were defined on the edges of the deck plate, except for the front side edge, considering the continuous existence of the deck plate in reality.

Comparisons between actual deck plate end and press-forming analysis results are shown in Figure 23, revealing that the deck plate's shape closely resembled the actual shape, successfully replacing the pressing process. Formation analysis of the deck end.

The outline and boundary conditions of the folding-up analysis are shown in Figure 24. The formation analysis of the deck end involved aligning a mold at a 90° angle to the deck, using the shape from the pressing analysis. The mold was modeled as a rigid body, with a chamfer radius of 2 mm to stabilize the contact between the deck and upper mold. Boundary conditions were set to ensure the lower mold was fully constrained, whereas the upper mold was constrained in all directions except for translation toward the deck plate. Symmetric boundary conditions were applied, considering the continuity of the deck at the nodes on both ends of the deck specimen. The length and angle of folds were set as 30 mm and 90°, respectively, as assumed in both impact and pull-out experiments.

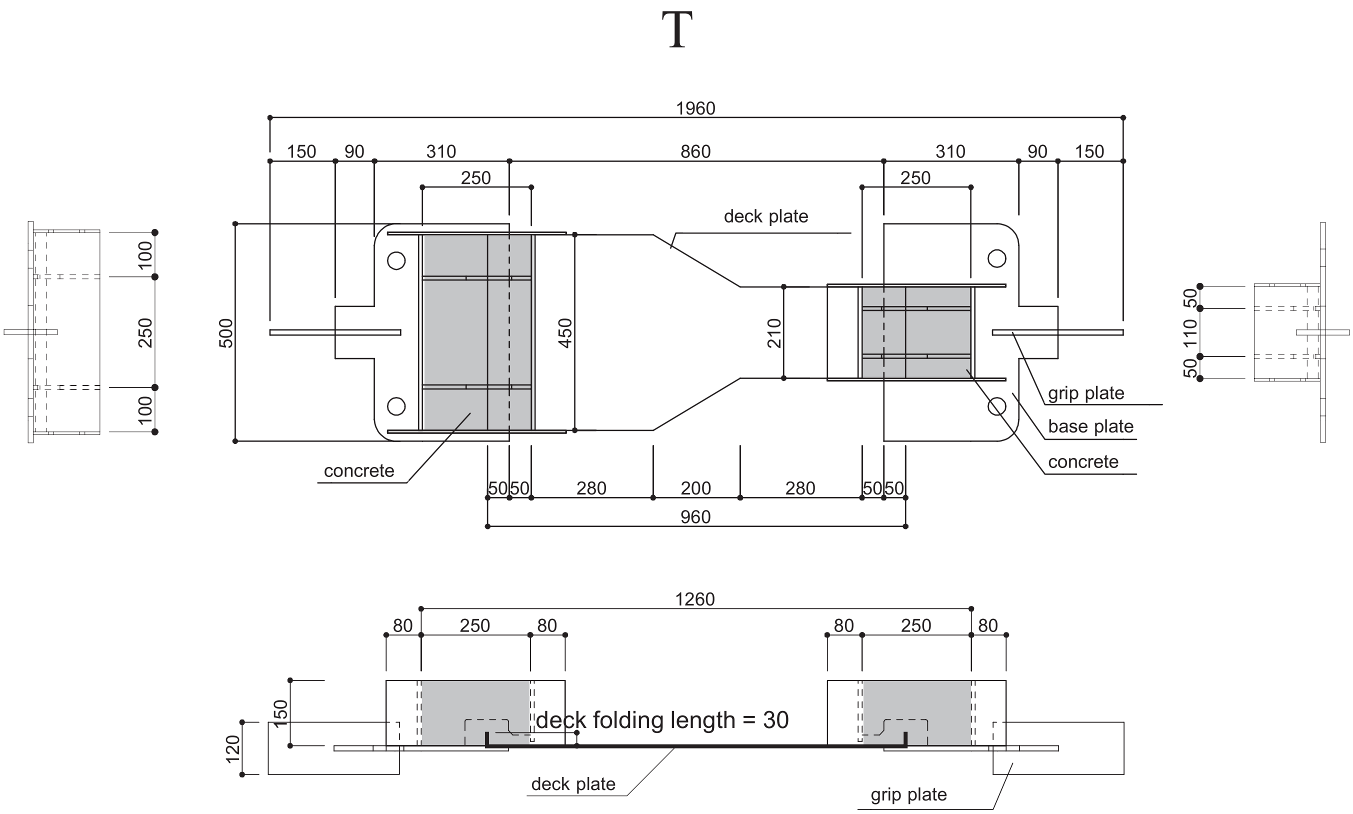

FIGURE 16 | Specimens of the pull-out experiment (mm).

TABLE 3 | Material test: (a) Deck plate, (b) concrete.

(a)			
Part	**Young modulus (MPa)**	**Yield stress (MPa)**	**Tensile strength (MPa)**
Deck plate	1.95×10^5	264	371
(b)			
Part	**Young modulus (MPa)**	**Compressive strength (MPa)**	**Split tensile strength (MPa)**
Concrete	2.58×10^4	21.2	1.96

A comparison between the folded-up deck end and shape obtained from the folding-up analysis is shown in Figure 25, demonstrating the successful replication of the bending-up process.

3.2.2 | Pull-Out Analysis of the Deck End

Two pull-out analyses were conducted to investigate the mechanical properties of anchoring systems. The first was a quasi-static analysis to validate the analysis model's ability to reproduce the static pull-out test (Pull-S). The second was a dynamic pull-out test that considered the increase in yield stress owing to the strain rate effect (Pull-D).

The pull-out analysis model, outlined in Figure 26, used rigid shell elements to model the concrete and the base plate. The rigid elements ensured a tight fit with the folded part, replicating the embedded condition in concrete. Forced displacement was imposed on the unfolded deck end.

When considering the strain rate effect, the Cowper-Symonds model expressed in Equation (4) [37] was utilized to account for the increase in yield stress resulting from this effect.

$$\sigma_y = \sigma_{y0}\left\{1 + (\dot{\varepsilon}/C)^{1/p}\right\} \tag{4}$$

where σ_y represents the yield stress considering the strain rate effect, σ_{y0} represents the initial yield stress, $\dot{\varepsilon}$ represents the strain rate, and C and p represent material constants. The values of $C=600$ and $p=3.5$ were determined based on the strain rate dependence of steels database established by Shimada [38]. In Pull-D, the pull-out duration was set to 0.05 s aligning with the impact time observed in the full-scale impact test conducted by Mizushima [12].

In Pull-S, where the strain rate was neglected, the deformation following the end of pulling is shown in Figure 27. The stretching of the folded deck plate end post-pulling, as shown in Figure 19,

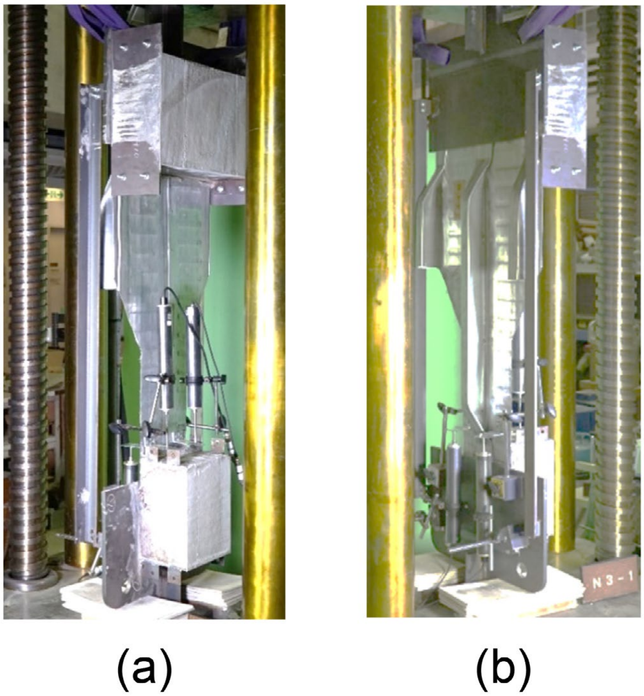

FIGURE 17 | Setup of the pull-out test: (a) Front side, (b) back side.

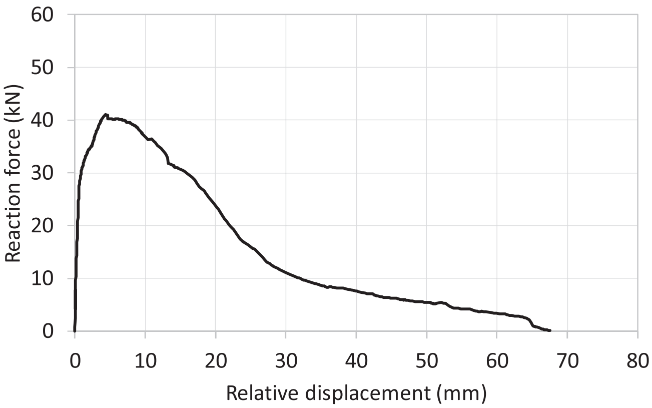

FIGURE 18 | Force-displacement diagram of the static pull-out test.

was successfully replicated in the analysis. Note that minimal disparity in the deformation appearance was noted even when accounting for the strain rate effect.

The relationship between pull-out displacement and reaction force is shown in Figure 28. The maximum load reached 41.04 kN in the experiment and 40.68 kN in the analysis, validating the accuracy of the analysis in reproducing the static experiment; although the slightly higher initial stiffness was observed in the analysis. The difference in the initial stiffness is attributed to the modeling assumption that the concrete block was idealized as a rigid body in the FE model. Furthermore, the analysis replicated the load-reduction behavior. In the analysis, it is considered that this somewhat rapid decrease in load was due to the deck tip not becoming completely flat, causing the residual bent portion to catch on the bent part of the shell element simulating the concrete. Additionally, in Pull-D, where the strain rate dependency was considered, the maximum strength increased to 66.5 kN, indicating an enhanced load capacity.

4 | FEA for Impact Test

In this section, we aim to replicate the damage conditions of the RC slab during a collision by analyzing the behavior of the anchor system through FEA.

4.1 | Analysis Model

The impact test analysis model, as depicted in Figure 29, utilized an 8-node hexahedron solid element to model the concrete of the slab. Each element was a reduced-integration type, featuring a single integration point at its center. The reinforcement bars and headed studs were represented by a 3-node beam element known as the Hughes–Liu beam [39]. One of the three nodes denotes the direction normal to the beam. The beam elements considered shear and bending deformations and shared nodes with the solid elements of the concrete, eliminating the bond-slip phenomenon between

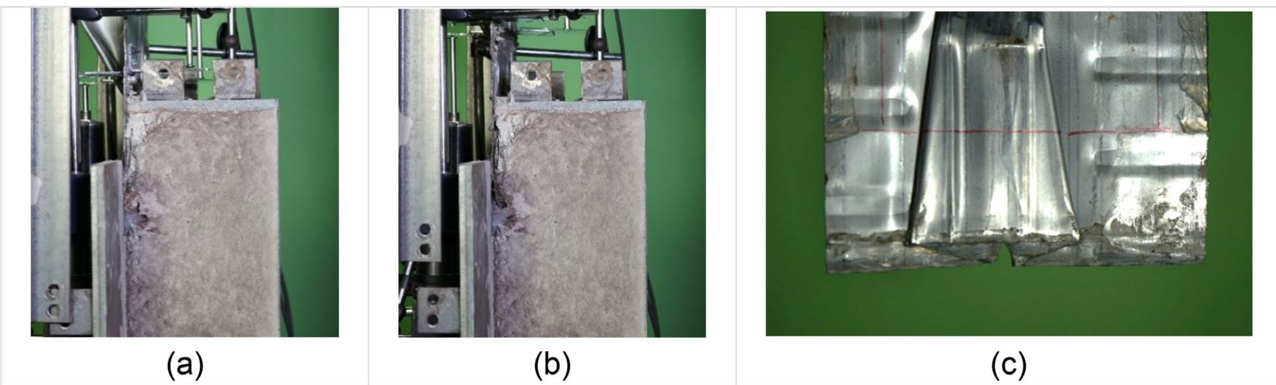

FIGURE 19 | Pull-out test conditions: (a) Concrete at maximum load, (b) concrete after test, (c) deck plate after test.

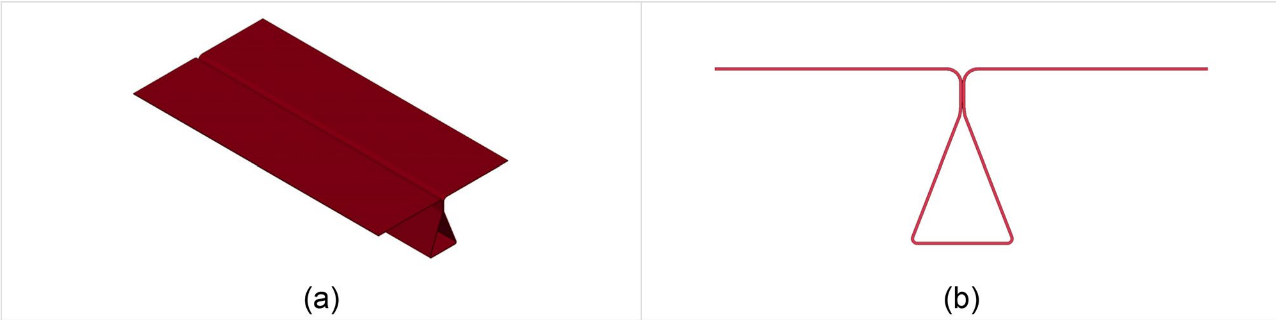

FIGURE 20 | Deck model before press forming: (a) Entire view, (b) section view.

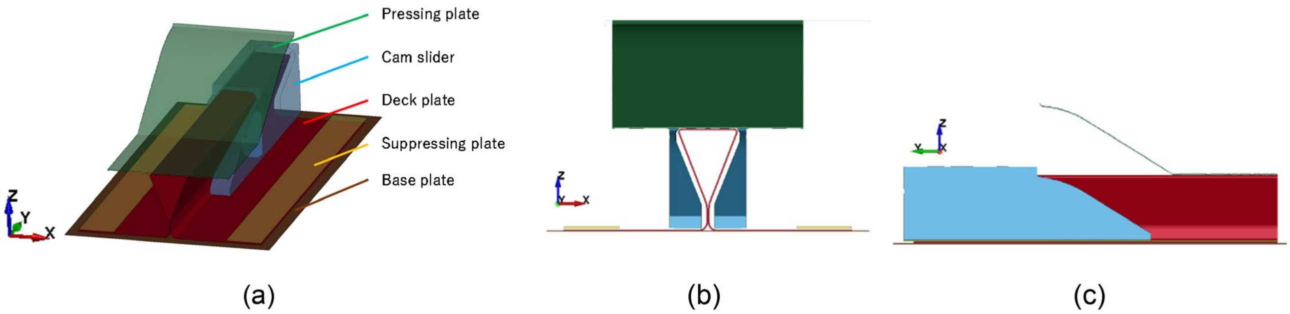

FIGURE 21 | Model for end pressing analysis: (a) Entire view, (b) front view, (c) side view.

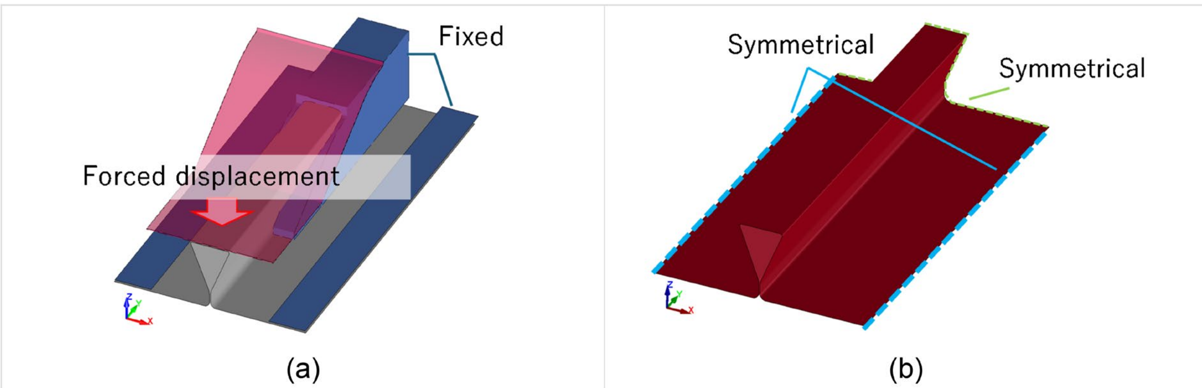

FIGURE 22 | Boundary conditions of pressing analysis: (a) Jigs, (b) deck plate.

the concrete and reinforcements. The RC slabs were modeled with a unit length of approximately 12.5 mm. This mesh size was selected based on existing literature dealing with slabs of similar thickness subjected to low-speed impact conditions [3, 6, 8, 11, 21, 24, 29, 31]. A mesh convergence study was not performed due to practical consideration; The finite element model included element eroding criterion, and changing the mesh size would necessitate recalibrating these criteria, potentially obscuring the modeling approach. As discussed in the results section, reasonable agreement was confirmed between the simulation outcomes and the experimental data, indirectly validating the chosen mesh size. A supplementary run for N-7.5 with a half-size mesh altered the peak penetration depth by approximately 5%, confirming mesh convergence. Steel beams were modeled using a 4-node Belytschko-Tsay shell element with one integration point in the plane and four integration points in the thickness direction. The twist-resistant joists were bolt-connected to the steel beams, with the bolt joints being represented by node sharing in the analysis. Steel deck plates were also modeled using shell elements. The screw connections between the ribs of the specimen were omitted. Instead, the adjacent nodes at the base of the ribs were shared. The concrete sections shared nodes with the headed studs, and these studs shared their bottom nodes with the shell flanges of the steel beams, effectively connecting the RC slabs with the steel beams. The total number of elements was 248 466.

In the FE model, contact conditions based on the penalty method [39] were utilized for the parts in which the separate members were in contact. Contact was defined between the projectiles and RC slab, projectiles and reinforcements, RC slab and steel beams, RC slab and deck plates, steel beams and deck plates, and among reinforcements. A friction coefficient of 0.3 was applied to both steel-steel and steel-concrete contacts

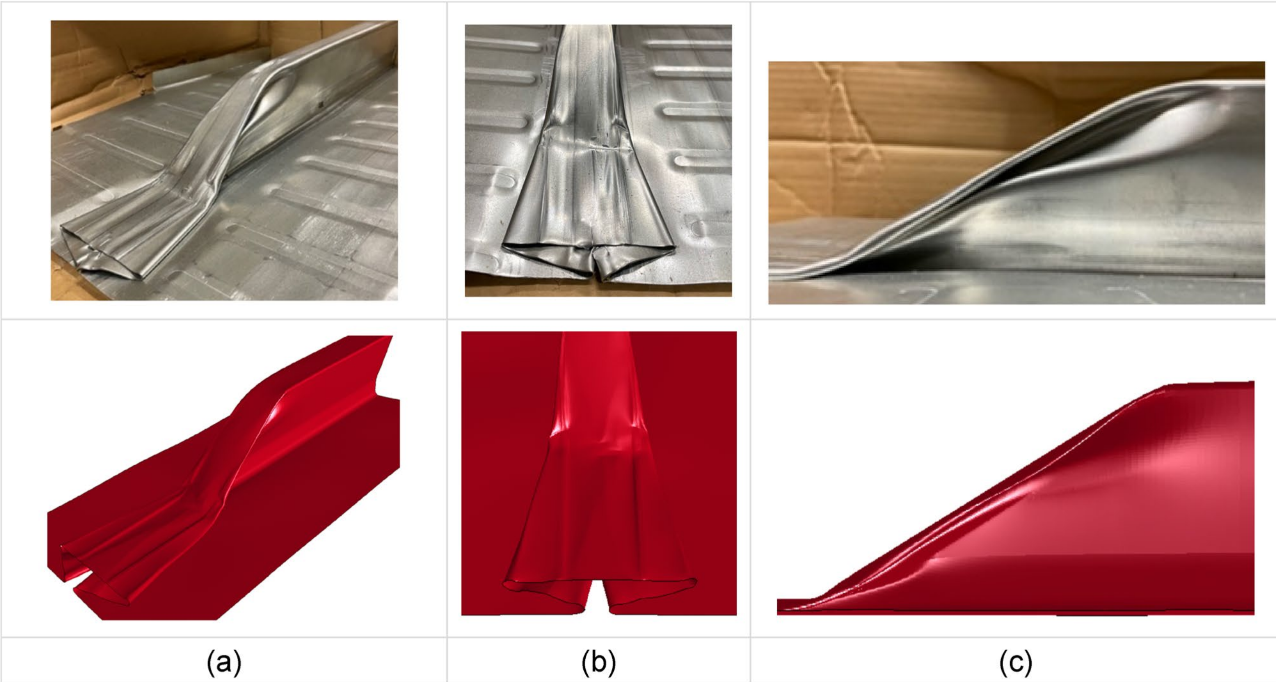

FIGURE 23 | Result of press-forming analysis: (a) Oblique, (b) front, (c) side.

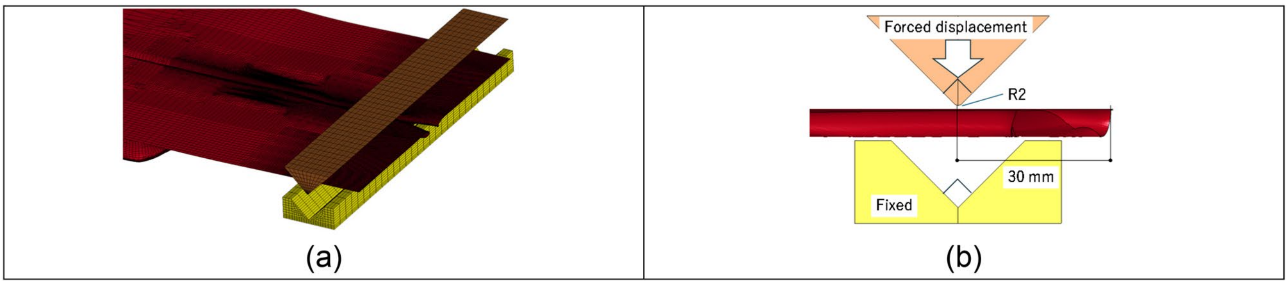

FIGURE 24 | Formation analysis model: (a) Outline, (b) detail of the deck end.

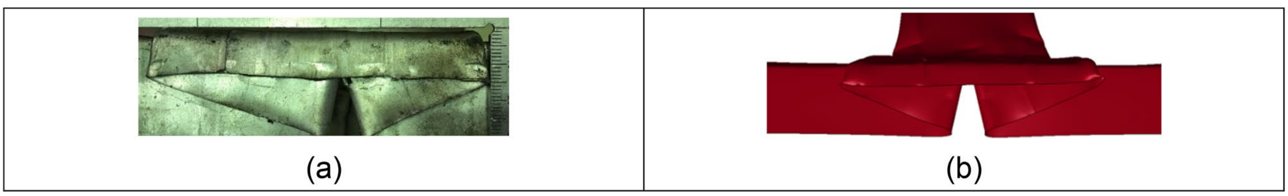

FIGURE 25 | Comparison of shapes after folding up: (a) Actual deck end, (b) analysis result.

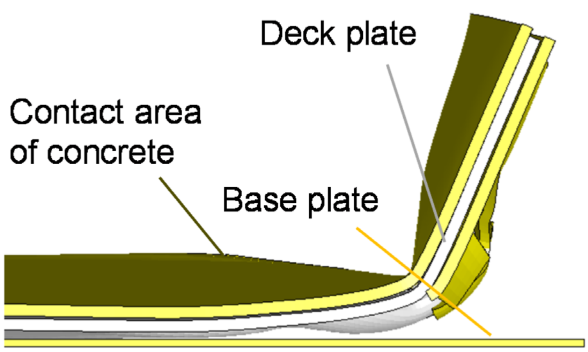

FIGURE 26 | Outline of the pull-out analysis model.

[40, 41]. Additionally, translation in the Z-direction, as shown in Figure 29a, was constrained at the location corresponding to the support point in the experiment.

The elastoplastic *MAT_WINFRITH_CONCRETE model, accounting for smeared crack behavior, was used for concrete components. Post-cracking stress–strain was modeled with linear softening [42, 43]. Compressive strength and Young's modulus were derived from material tests in Table 1, while tensile strength was calculated using Equation (5) from the AIJ Standards for Structural Calculation of Reinforced Concrete Structures [44].

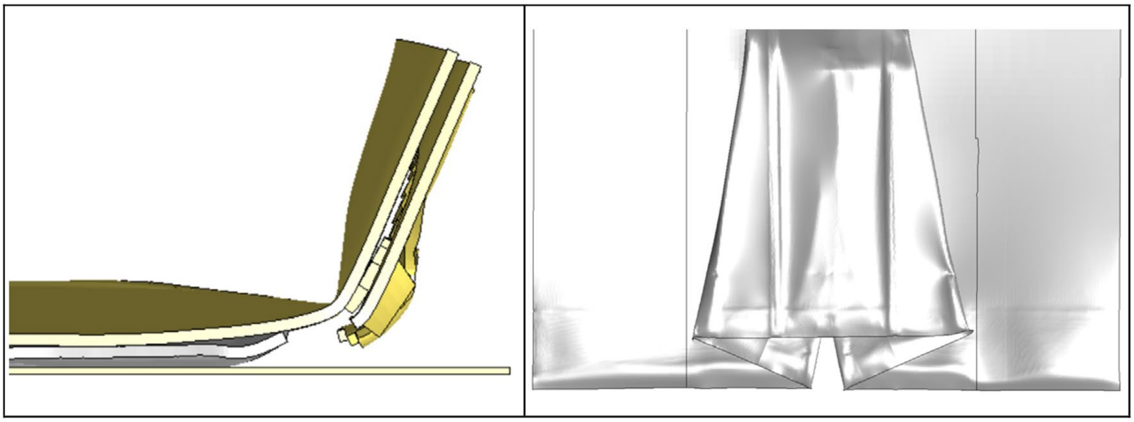

FIGURE 27 | Deformation of the anchor system after pull-out.

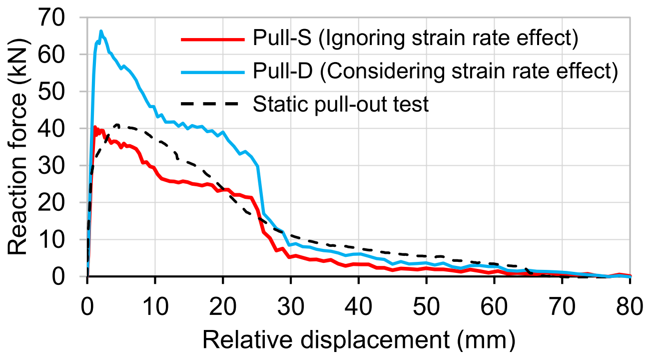

FIGURE 28 | Force–displacement relationship of pull-out analysis.

$$f_t = 0.56\sqrt{\sigma_b'} \tag{5}$$

where σ_b' represents the compressive strength of the concrete.

The complete crack opening width, w, corresponding to zero stress, was determined from G_f, which is the fracture energy of concrete per unit crack area. G_f was calculated from the maximum aggregate diameter, $d_{\max}$, and uniaxial compressive strength of concrete, σ_b' based on Equation (6) specified in the standards specification for concrete structures 2012 [45].

$$w = \frac{2G_f}{f_t}, G_f = 10\sigma_b'^{\frac{1}{3}} \cdot d_{\max}^{\frac{1}{3}} \tag{6}$$

The concrete model was considered to be a failure criterion specified by the maximum principal strain and shear strain using *MAT_ADD_EROSION. The failure maximum principal strain of 0.04 and maximum shear strain of 0.045 were determined through a trial-and-error process to accurately replicate the damage conditions observed in the experimental RC slab.

The reinforcement bars were assumed to be elastoplastic with strain rate dependence based on the Cowper-Symonds equation and the deck plate in the pull-out analysis. The stress–strain relationship was approximated by a multilinear approximation based on material test results shown in Table 1, and this behavior was modeled using *MAT_PIECEWISE_LINEAR_PLASTICITY. The limit of element deletion was set to 0.2 of the equivalent plastic strain to express the failure of the reinforcement bars. The ultimate elongation of the reinforcing bars could not be determined from the material test because all three tensile coupons fractured outside the punched gauge marks, making post-fracture extension unmeasurable. Therefore, fracture criteria were established based on [12]. The bilinear elastoplastic model *MAT_PLASTIC_KINEMATIC was utilized for other steel parts, such as the deck plate, steel beam, joist, and projectile. The material parameters were also determined based on the material test shown in Table 1.

For the F-series analysis, a dislodgement model was proposed to replicate the anchoring system at the deck ends, based on shear stress between the concrete and the deck end. The folded-up shape of the deck ends was not explicitly modeled. A linear softening model was adopted after reaching the shear criterion, as shown in Figure 30, to represent the relationship between shear stress and displacement. The displacement shown in Figure 30 was scaled by half to accommodate the specimen's scale. The maximum strength of the anchoring system was calculated based on the maximum load obtained from the pull-out analysis and the contact area of the deck plate.

4.2 | Results of the Impact Analysis

A summary of the analysis results is presented in Table 4, with time histories of the falling velocities of the projectiles and penetration depths shown in Figures 31 and 32, respectively. Figures 33 and 34 illustrate the states of the damaged RC slab and the dislodgement of the deck plate ends, respectively. The analysis demonstrated the local failure of RC slabs, consistent with the experimental observations. The analysis reproduced the deck detachment behavior observed at a fall height of 13 m; successfully capturing the detachment without the anchoring system and the prevention of detachment with the system in place.

In N-7.5, reinforcement failure was not observed, similar to the experiment. The projectile's velocity aligned with the experimental results. The deck ends were dislodged on both sides,

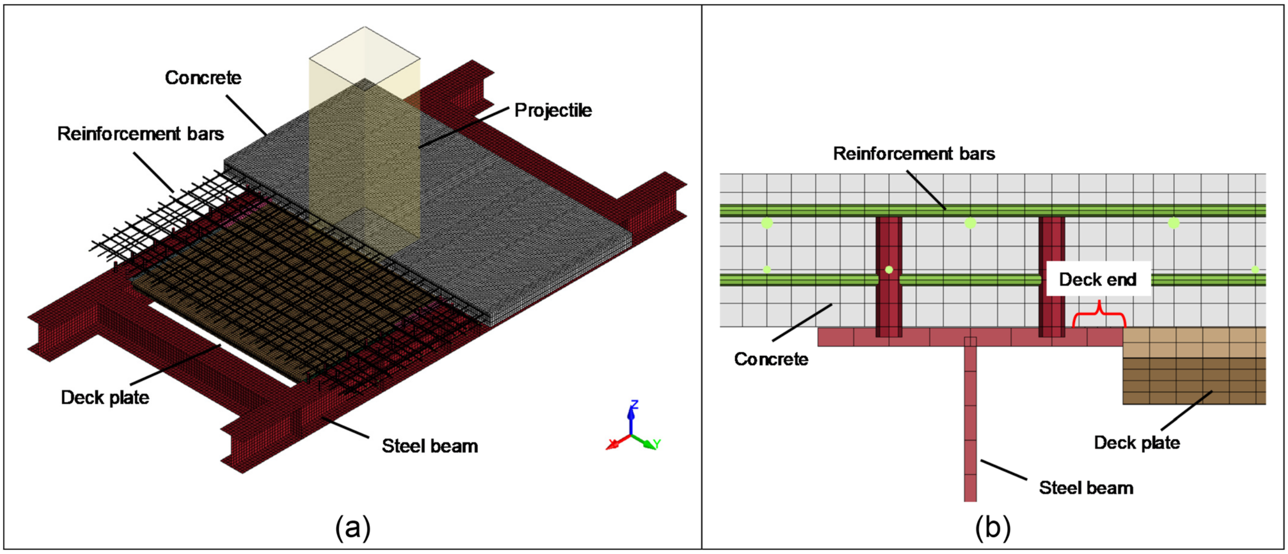

FIGURE 29 | Analysis model: (a) Complete view, (b) close view.

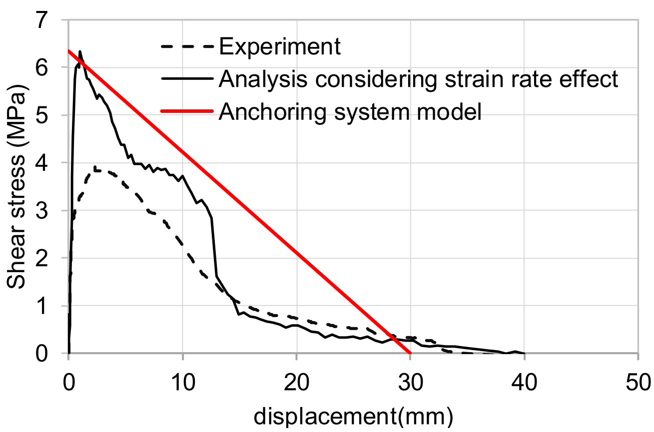

FIGURE 30 | Analysis model.

leaving approximately half of their length intact, although the penetration depth closely mirrored the experimental results. In N-9, dislodgement was not observed in the analysis, which slightly underestimated the penetration depth. A few upper reinforcement bars failed, similar to the experiment. The projectile velocity almost aligned with that obtained experimentally. In N-13, the deck plate was completely dislodged, similar to the experiment. While seven reinforcements failed in the experiment, the analysis showed three upper and one lower reinforcement failure. The projectile velocity and penetration depth were reproduced in the analyses.

In F-13, the detachment of the deck plates was successfully suppressed by applying the proposed mechanical model for the anchoring system, aligning with the experimental results. The time histories of the projectile velocity and penetration depth closely matched the experimental data, indicating the validity of the shear dislodgement model of the anchoring system. However, the analysis slightly overestimated the number of failed reinforcement bars. In F-14, the analysis reproduced the state of debris scattering and detachment from the deck plate. The time history of the projectile velocity closely matched the experimental results. However, the analysis overestimated the penetration depth. This is probably because while no reinforcement bar failures were observed in the experiment, the analysis predicted the failure of two bars, indicating an overestimation in the number of failed reinforcement bars. This discrepancy may be attributed to the difference in impact angle; the analysis assumed a vertical impact, whereas the experiment involved a slightly oblique impact. The oblique impact in the experiment could have resulted in less penetration depth and fewer reinforcement bar failures due to the distribution of impact energy in different directions. In F-15, the deck plates detached in the analysis, similar to the experimental observations. However, while the experiment observed over 10 reinforcement bar failures, the analysis predicted only two, indicating an underestimation. This likely contributed to the underestimated penetration depth. The fracture elongation, unavailable from material tests, and reliance on reference values may have caused the discrepancy in reinforcement bar failures.

5 | Conclusions

This study proposed an anchoring system for steel deck plates to prevent debris scattering of RC slabs under low-velocity impacts. A half-scale impact test was conducted to assess the effectiveness of this mitigation strategy. Component tests and FEA were performed to thoroughly investigate the mechanical properties of the anchoring system. Furthermore, an impact analysis was conducted by considering the pulling out of the anchoring system using the results of the component test and analysis. The study's findings include:

- In contrast to conventional strengthening approaches relying on high-performance materials or adhesively bonded reinforcements—often entailing elevated costs and complex installation—the present method utilizes commonly used deck plates as integral protective elements. The proposed system effectively prevented debris scattering under impact conditions. Debris scattering occurred at a fall height of

TABLE 4 | Summary of impact analysis.

		N-series			F-series		
		N-7.5	**N-9**	**N-13**	**F-13**	**F-14**	**F-15**
Deck falling	Exp.	Present	Present	Present	Absent	Absent	Present
	Ana.	Absent	Absent	Present	Absent	Absent	Present
Number of failed rebars	Exp.	None	1	7	1	0	Over 10
	Ana.	None	2	4	3	2	2

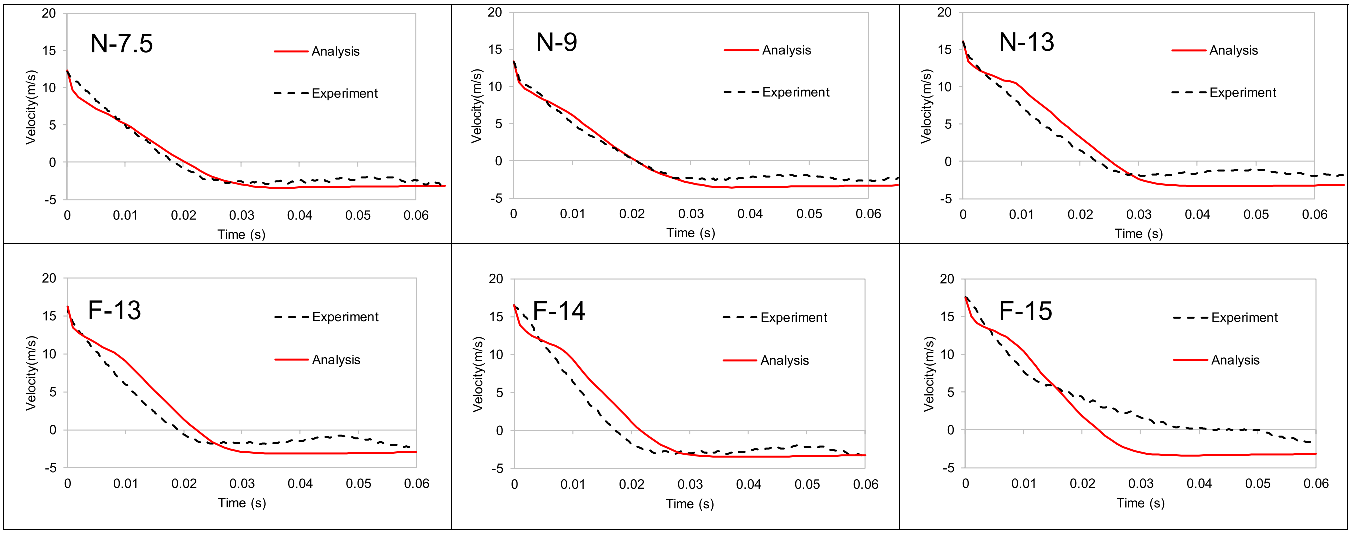

FIGURE 31 | Projectile velocity.

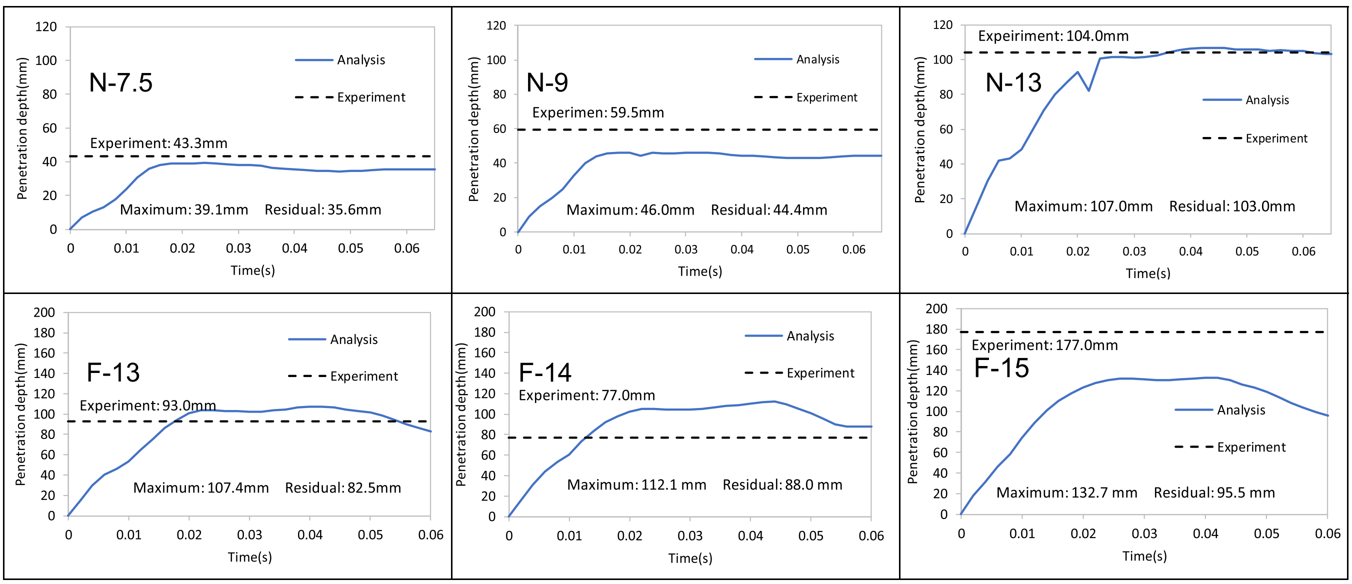

FIGURE 32 | Penetration depth.

7.6 m without the anchor system, consistent with previous studies, which demonstrated that deck detachment occurs when the impact condition is beyond the perforation limit proposed by Degen. By contrast, the proposed anchoring system successfully suppressed debris scattering up to a fall height of 13.9 m.

- A static component pull-out test of the anchoring system was performed; the maximum strength was 41 kN, followed by a gradual load decrease, resulting in full pull-out. The deck plate was fully elongated after pull-out, with the maximum strength likely influenced by the behavior of the folded deck plate. Numerical analysis was

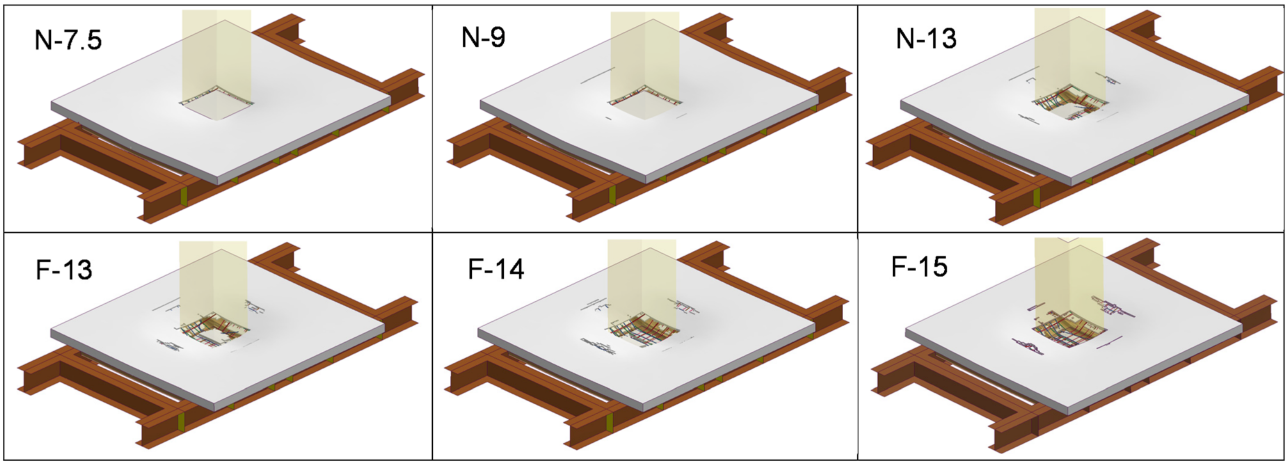

FIGURE 33 | States of damaged RC slabs.

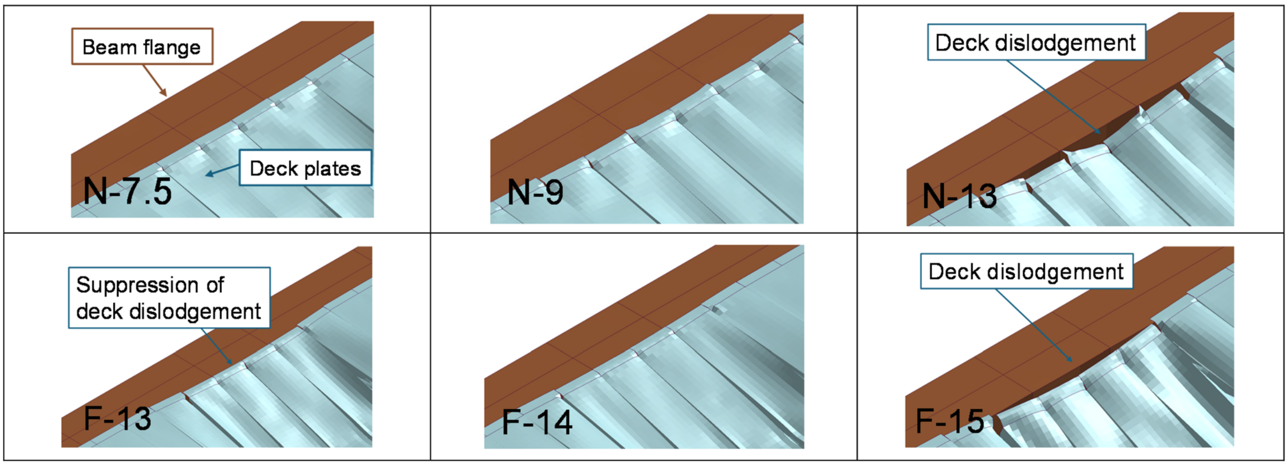

FIGURE 34 | Dislodgements of deck ends.

conducted by replicating the anchoring system's shape through FEA of processing procedures, resulting in a 60% increase in pull-out strength by considering strain rate effects.

- Impact analysis successfully reproduced the state of deck plate detachment by incorporating the anchorage model developed from the pull-out test and analysis, with N-13 and F-13 analyses accurately reflecting the presence or absence of these occurrences depending on whether the anchoring system was applied. However, the numerical analysis still has limitations in accurately predicting deck plate detachment in cases without the anchoring system. Furthermore, the F-15 analysis underestimated the failure of reinforcement bars and penetration depth, despite accurately reproducing deck plate detachment in F-series, likely resulting from a lack of rupture elongation data from material tests. Although the FEA effectively predicted deck plate detachment, its precision in cases of multiple reinforcement bar failures was inadequate.

The anchored steel deck plate system offered a practical and cost-effective solution for enhancing the impact resistance of RC slabs. By utilizing steel deck plates that are commonly used in construction as permanent formwork, our proposed system can be implemented with minimal cost and construction time. Its scalability and straightforward application make it a viable option for large-scale construction projects. This is particularly advantageous for urban construction projects where prioritizing the safety of construction workers and public thoroughfares is crucial. Future investigations will focus on developing a predictive method for debris scattering without relying on FEA through a more detailed theoretical exploration of the load transfer mechanism. While this study addressed a general slab configuration, further research could examine the adaptability of the proposed system to various slab specifications. Because a specimen struck at a slightly oblique angle (F-14) showed a smaller penetration depth than the nearly vertical case, vertical impact can be regarded as the critical scenario; controlled oblique-angle tests are planned for future work. Furthermore, recent advances in vision-based crack tracking and debris-trajectory measurement will be explored as a potential extension of this work.

Conflicts of Interest

The authors declare no conflicts of interest.

Data Availability Statement

Data sharing not applicable to this article as no datasets were generated or analyzed during the current study.

References

1. C. Ito, H. Onuma, and K. Shirai, *Design Method of Concrete Structures Against Impact due to Collision of Missile, Report of Central Research Institute of Electric Power Industry, U24* (Central Research Institute of Electric Power Industry, 1991) (In Japanese).

2. P. Degen, "Perforation of Reinforced Concrete Slabs by Rigid Missiles," *Journal of the Structural Division, ASCE* 106, no. 7 (1980): 1623–1642.

3. S. Şengel, H. Erol, T. Yılmaz, and Ö. Anıl, "Investigation of the Effects of Impactor Geometry on Impact Behavior of Reinforced Concrete Slabs," *Engineering Structures* 263 (2022): 114429.

4. Y. Xiao, B. Li, and K. Fujikake, "Behavior of Reinforced Concrete Slabs Under Lowvelocity Impact," *ACI Structural Journal* 114, no. 3 (2017): 643–658.

5. F. Wang, J. B. Liu, X. Bao, S. T. Li, and Z. Y. An, "Experimental Study of the Resistance of RC Walls With Different Transverse Reinforcements Subjected to Large-Scale Rigid Projectile Impacts," *Engineering Structures* 251, no. Part B (2022): 113558.

6. Z. Wang, C. Hou, and Q. Guo, "Numerical Simulation on the Dynamic Response of Bonded Unidirectional Prestressed Concrete Slabs Subjected to Low-Velocity Impact," *Structure* 38 (2022): 1098–1110.

7. A. I. Said and E. M. Mouwainea, "Experimental Investigation on Reinforced Concrete Slabs Under High-Mass Low Velocity Repeated Impact Loads," *Structure* 35 (2022): 314–324.

8. T. Yılmaz, N. Kıraç, Ö. Anil, R. T. Erdem, and G. Kaçaran, "Experimental Investigation of Impact Behaviour of RC Slab With Different Reinforcement Ratios," *KSCE Journal of Civil Engineering* 24 (2020): 241–254.

9. K. Vimal, M. A. Iqbal, and A. K. Mittal, "Experimental Investigation of Prestressed and Reinforced Concrete Slabs Under Falling Weight Impactor," *Thin-Walled Structures* 126 (2018): 106–116.

10. K. Vimal, M. A. Iqbal, and A. K. Mittal, "Study of Induced Prestress on Deformation and Energy Absorption Characteristics of Concrete Slabs Under Drop Impact Loading," *Construction and Building Materials* 188 (2018): 656–675.

11. M. A. Iqbal, K. Vimal, and A. K. Mittal, "Experimental and Numerical Studies on the Drop Impact Resistance of Prestressed Concrete Slabs," *International Journal of Impact Engineering* 123 (2019): 98–117.

12. Y. Mizushima, Y. Horiuchi, K. Haraguchi, I. Hosokawa, and W. Oba, "Study on Behavior of Reinforce Concrete Slabs Subjected to Impact of Accidentally Falling Objects During Construction," *Journal of Structural and Construction Engineering (Transactions of AIJ)* 83, no. 751 (2018): 1239–1249. (in Japanese).

13. Y. Mizushima and N. Iino, "Behavior of Thin Reinforced Concrete Slabs and Effect of Reinforcement Bars Subjected Low-Velocity Impact," *Structure* 38 (2022): 832–847.

14. H. Othman and H. Marzouk, "Impact Response of Ultra-High-Performance Reinforced Concrete Plates," *ACI Structural Journal* 113, no. 6 (2016): 1325–1334.

15. B. Batarlar, M. Hering, F. Bracklow, T. Kühn, B. Beckmann, and M. Curbach, "Experimental Investigation on Reinforced Concrete Slabs Strengthened With Carbon Textiles Under Repeated Impact Loads," *Structural Concrete* 22 (2020): 120–131.

16. M. Beppu, A. Ogawa, and J. Takahashi, "Impact Resistant Performance of Fiber Reinforced Cementitious Composite Plates Subjected to High Velocity Impact by a Rigid Projectile," *Journal of Japan Society of Civil Engineers, Ser. E2 (Materials and Concrete Structures)* 70, no. 2 (2014): 180–193.

17. D. Elavarasi and R. M. K. Saravana, "On Low-Velocity Impact Response of SIFCON Slabs Under Drop Hammer Impact Loading," *Construction and Building Materials* 160 (2018): 127–135.

18. A. B. Elnagar, H. M. Afefy, A. T. Baraghith, and M. H. Mahmoud, "Experimental and Numerical Investigations on the Impact Resistance of SHCC-Strengthened RC Slabs Subjected to Drop Weight Loading," *Construction and Building Materials* 229 (2019): 116866.

19. M. Mastali, N. M. Ghasemi, M. Naghipour, and S. M. Rabiee, "Experimental Assessment of Functionally Graded Reinforced Concrete (FGRC) Slabs Under Drop Weight and Projectile Impacts," *Construction and Building Materials* 95 (2015): 296–311.

20. G. H. Heo, J. G. Park, and C. G. Kim, "Evaluating the Resistance Performance of the VAEPC and the PAFRC Composites Against a Low-Velocity Impact in Varying Temperature," *Advances in Civil Engineering* 2020 (2020): 7901512.

21. S. M. Anas, M. Shariq, M. Alam, A. M. Yosri, A. Mohamed, and M. AbdelMongy, "Influence of Supports on the Low-Velocity Impact Response of Square RC Slab of Standard Concrete and Ultra-High Performance Concrete: FEM-Based Computational Analysis," *Buildings* 13 (2023): 1220.

22. P. B. Sakthivel, A. Ravichandran, and N. Alagamurthi, "Impact Strength of Hybrid Steel Mesh-And-Fiber Reinforced Cementitious Composites," *KSCE Journal of Civil Engineering* 19 (2015): 1385–1395.

23. T. Almusallam, Y. Al-Salloum, S. Alsayed, R. Iqbal, and H. Abbas, "Effect of CFRP Strengthening on the Response of RC Slabs to Hard Projectile Impact," *Nuclear Engineering and Design* 286 (2015): 211–226.

24. T. Yılmaz, N. Kıraç, Ö. Anil, R. T. Erdem, and C. Sezer, "Low-Velocity Impact Behaviour of Two Way RC Slab Strengthening With CFRP Strips," *Construction and Building Materials* 186 (2018): 1046–1063.

25. H. Mikami, N. Kishi, T. Ando, and Y. Kurihashi, "Experimental Study on Impact Resistance of RC Slabs Strengthened With FRP Sheet," *Journal of Structural Engineering* 48A (2002): 1531–1542.

26. S. Kiyota, S. Kataoka, M. Beppu, H. Ichino, and K. Sato, "Mitigation Effect by Aramid Fiber Sheets Reinforcement on the Scabbing of RC Slabs," *Journal of Structural Engineering* 66A (2020): 1047–1058.

27. S. J. Yoo, T. F. Yuan, S. H. Hong, and Y. S. Yoon, "Effect of Strengthening Methods on Two-Way Slab Under Low-Velocity Impact Loading," *Materials* 13 (2020): 5603.

28. M. Loganaganandana, G. Murali, M. P. Salaimanimagudam, M. K. Haridharan, and K. Karthikeyan, "Experimental Study on GFRP Strips Strengthened New Two Stage Concrete Slabs Under Falling Mass Collisions," *KSCE Journal of Civil Engineering* 25 (2021): 235–244.

29. H. S. Şengel, H. Erol, T. Yılmaz, Ö. Anıl, H. C. Gürdal, and A. M. Uludoğan, "Low-Velocity Impact Behavior of Two-Way RC Slab Strengthening With Carbon TRM Strips," *Structure* 44 (2022): 1695–1714.

30. Z. Wang, J. Yan, Y. Lin, F. Fan, and M. Sun, "Experimental and Analytical Study on the Double Steel Plates-UHPC Sandwich Slabs Under Low-Velocity Impact," *Thin-Walled Structures* 184 (2023): 110548.

31. H. Soltani, A. Khaloo, and H. Sadraie, "Dynamic Performance Enhancement of RC Slabs by Steel Fibers vs. Externally Bonded GFRP Sheets Under Impact Loading," *Engineering Structure* 213 (2020): 110539.

32. T. Almusallam, H. Abas, O. Hodali, N. Siddiqui, and Y. Al-Salloum, "Behavior of Prestressed Fiber-Reinforced Steel-Lined Concrete Slabs Under Projectile Impact," *Archives of Civil and Mechanical Engineering* 23 (2023): 64.

33. R. P. Kennedy, “A Review of Procedures for the Analysis and Design of Concrete Structure to Resist Missile Impact Effect,” *Nuclear Engineering and Design* 37 (1976): 183–203.

34. K. Muto, “Experimental Studies on Local Damage of Reinforced Concrete Structures by the Impact of Deformable Missiles Part 1—Outline of Test Program and Small-Scale Tests,” *Transaction of the 10th International Conference on Structural Mechanics in Reactor Technology* J (1989): 257–264.

35. Y. Esashi, H. Ohnuma, C. Ito, and K. Shirai, “Experimental Studies on Local Damage of Reinforced Concrete Structures by the Impact of Deformable Missiles Part 2—Intermediate Scale Tests,” *Transaction of the 10th International Conference on Structural Mechanics in Reactor Technology* J (1989): 265–270.

36. K. Muto, T. Sugano, H. Tsubota, et al., “Experimental Studies on Local Damage of Reinforced Concrete Structures by the Impact of Deformable Missiles Part 3—Full Scale Tests,” *Transaction of the 10th International Conference on Structural Mechanics in Reactor Technology* J (1989): 271–278.

37. G. R. Cowper and P. S. Symonds, *Strain Hardening and Strain Rate Effects in the Impact Loading of Cantilever Beams* (Brown University, Applied Mathematics Report, 1958).

38. Y. Shimada, “Database of Steel Hysteretic Characteristics Affected by Strain-Rate,” *Proceedings of Constructional Steel* 20 (2012): 1–8.

39. ANSYS, Inc, LS-DYNA R15 Theory Manual, https://lsdyna.ansys.com/manuals/.

40. H. Charsetad and S. M. Khorsandijou, “Effect of Surface Roughness on Steel-Steel Dry Friction Coefficient,” *Journal of Mechanics Research and Application* 4, no. 3 (2012): 45–56.

41. W. Zhao and B. Zhu, “Theoretical Model for the Bond–Slip Relationship Between Ribbed Steel Bars and Confined Concrete,” *Structural Concrete* 19, no. 2 (2017): 548–558.

42. B. J. Broadhouse and A. J. Neilson, “Modelling Reinforce Concrete Structure in DYNA3D,” *AEE Winfrith* (1987): AEEW-M 2465.

43. B. J. Broadhouse, *The Winfrith Concrete Model in LS-DYNA3D, Report: SPD/D(95)3* (Structural Performance Department, AEA Technology, Winfrith Technology Centre, 1995).

44. Architectural Institute of Japan, *AIJ Standard for Structural Calculation of Reinforced Concrete Structure* (AIJ, 2018).

45. Japan Society of Civil Engineering, *Standard Specifications for Concrete Structure—2012, Design* (Japan Society of Civil Engineering, 2012).